ORIGINAL ARTICLE

Enhancing the tribological performance of polymeric laminated composite materials by adopting the functionally graded materials technique

Mostafa A. A. Nowier[1] · Amr A. Abd-Elhady[1] · Hossam El-Din M. Sallam[2] · Mahmoud Atta[3]

Received: 5 November 2024 / Revised: 9 March 2025 / Accepted: 4 May 2025 / Published online: 20 May 2025
© The Author(s) 2025

Abstract
The concept of functionally graded materials was adopted to experimentally enhance the wear resistance and hardness of the traditional laminated composite materials made of long glass fibers and epoxy resin in this work. The laminated composite structure consisted of twelve layers. The redistribution of fibers through the width of the specimens produces three distinct functionally graded patterns: linear, non-linear, and stepwise. A Shore-D hardness tester was used to get the hardness of each pattern, while their wear and friction coefficients were measured through a Pin-On-Disc tester according to ASTM standards for applied load varied from 10 to 40 N and sliding speed ranged from 0.2 to 0.8 m/s. The study also considered the effects of fiber orientation relative to the sliding direction, i.e., parallel, anti-parallel, and normal. The worn surfaces of the composite were inspected using an optical microscopy microscope, X-ray diffraction analysis, and scanning electron microscope. The results indicated that the wear rate, friction coefficient, and temperature of a functionally graded composite are influenced by several factors, including sliding speed, applied load, sliding distance, and fiber orientation. The composite demonstrated superior wear performance in the normal orientation compared to parallel and anti-parallel ones. The linear patterns improved the wear resistance rate and coefficient of friction of conventional composites with an average of 15% and 3%, respectively, in the normal orientation in all manners of applied forces and sliding velocities. Meanwhile, the stepwise patterns enhanced both of them by up to 25% and 8% in parallel and anti-parallel orientations for the same cases.

Keywords Functionally graded composite (FGC) · Fiber orientations · Hardness · Abrasive wear loss · Coefficient of friction · Tribological properties

1 Introduction

Polymeric composite materials are extensively utilized in engineering applications [1]. Mechanical and automotive industries continuously seek materials capable of withstanding the abrasive impacts of particles such as sand and silicon carbide. Research indicates that approximately 60% of polymer composite failures result from abrasion wear [2]. Abrasive wear is notably significant, accounting for around 50% of total wear [3] and approximately 63% of the total wear-related costs [4]. Therefore, researchers have spatially changed the traditional microstructure of composites according to the application of understudied material to improve its behavior, which is known as

functionally graded composite materials (FGCs). The characteristics of such FGCs vary according to the reinforcement direction and percentages through the structure. FGCs improve the properties of classical composite materials [5] and enhance attributes such as hardness and wear resistance [6]. So, functionally graded fibrous composites were developed to overcome the shortcomings of polymeric composite materials [7].

Particle-reinforced composites, widely used in wear-resistant applications, offer cost-effectiveness and ease of manufacturing [8]. Researchers have incorporated different types of fillers into polymers to enhance these properties. The resulting composites exhibit significantly improved mechanical performance compared to unmodified polymers [9]. Based on the filler geometry, they are classified into three types: 0-D (dot or spherical shapes), 1-D (rod-like or fibrous structures), and 2-D (sheet-like or layered formations) [10]. Sahu et al. [11] investigated and predicted the mechanical properties of nanocomposites made from high-density polyethylene (HDPE) reinforced with nanodiamonds. Pradeep et al. [12] fabricated basalt fiber-reinforced composites incorporating silicon dioxide (SiO_2) nanofillers, improving mechanical properties, hardness, and wear resistance. Saleh et al. [13] reused magnesium chips to produce gradient composites reinforced with silicon carbide to improve the wear characteristics. Song et al. [14] reviewed the factors affecting the wear behavior of polymeric materials, including lubrication, material composition, load, speed, impact angle, abrasive particles, and temperature. They concluded that modifying material formulation ratios can significantly influence properties like hardness, which, along with hydrophilicity, impacts wear resistance and lubrication performance. Babu et al. [15] investigated the development of hybrid composites using AA 2014 alloy reinforced with Zirconium Diboride (ZrB_2) and Boron Carbide (B_4C). They enhanced hardness, tensile strength, and wear resistance by employing liquid metallurgy stir casting and varying reinforcement weight percentages.

The abrasion significantly impairs polymeric composites' strength and wear behavior. It can be recognized as a critical issue that can degrade the performance of polymer composites. Numerous studies have been conducted with a focus on the effects of abrasion under both single and multi-pass conditions. Mohan et al. [16] examined the two-body abrasive wear behavior of glass fabric-epoxy (GE) composites reinforced with silicon carbide (SiC). Their study showed a notable decrease in wear loss and specific wear rates with the addition of SiC filler. Chairman et al. [17] studied the abrasive wear of basalt fabric-epoxy composites (BE) under varying loads and constant velocity. They found that basalt fabric reinforcement significantly improved wear resistance, outperforming polyester-reinforced basalt fibers. The study highlighted the importance of reinforcement geometry in achieving better wear resistance. Suresha et al. [18] found that the wear resistance of polymer composites was affected by the type of used fibers, i.e., carbon fibers offered superior resistance over glass ones.

As is already known, fiber direction is a crucial factor in calculating the properties of composites. Most of them have focused on two approaches to study the effect of fiber orientation on friction and wear properties according to the sliding direction. Through the first one, fibers are oriented either normal (N-O), parallel (P-O), or anti-parallel (AP-O) to the sliding directions. The other is fibers that are randomly or unidirectionally oriented. For the oriented one, some findings are contradictory. For instance, Alshammari et al. [19] reported that the AP-O offered the best tribological behavior, followed by P-O and N-O [20, 21]. Conversely, other studies found that the P-O provided superior wear resistance [22, 23], while additional research indicated that the N-O was most effective [24, 25].

Gautam et al. [26] found that abrasive medium and fiber fraction were the most critical factors in wear tests, while normal load had minimal impact. In contrast, Singh et al. [27] compared homogeneous fiber distribution with FGMs in vinyl ester composites reinforced with Kevlar (5 wt%) and varying bagasse fiber content (0–15 wt%). They identified normal load as the most significant factor affecting sliding behavior, differing from Gautam's[26] findings, likely due to the use of different reinforcements. Jojith et al. [28] have shown that speed, sliding time, applied load, thermal conditions, radial distance, and reinforcement type are the most significant factors influencing the tribological behavior of wear abrasives. A study on a composite of unidirectional E-glass fiber-reinforced epoxy, using the pin-on-ring technique, examined friction and wear properties. The findings indicated that increasing sliding under clean and wet conditions enhances the friction coefficient and wear rate [29]. Gangil et al. [30] compared homogeneously distributed fiber composites and functionally graded material (FGM) fiber composites, revealing the superior performance of FGM fiber composites. Singh et al. [31] found that the mechanical properties of FGCs were more sensitive

to the effect of the fiber volume fraction (V_f %) than homogeneous composites. Boggarapu et al. [32] fabricated Al/Cu functionally graded material using powder sintering, achieving robust interfacial bonding between graded layers. This enhanced the material's strength, inhibited crack propagation, and resulted in superior friction and wear properties compared to the base materials. Prakash et al. [33] investigated the tribological properties of epoxy composites reinforced with various stacking sequences of abaca (A) and glass (G) fibers (AAAA, AGAG, AGGA, and GAAG). Their findings revealed that incorporating glass and abaca fibers significantly enhanced the composites' resistance to abrasive wear, with the AGGA hybrid composite demonstrating the lowest wear rate. Alhazmi et al. [34] found that increasing the average V_f % to 22% of FGCs and layers number improves their wear resistance.

The primary objective of the present research is to enhance the tribological behavior of traditional composites by introducing FG laminated composites with the same V_f%. This objective is achieved by evaluating the tribological performance of both FGs and conventional composites in addition to examining the impact of fiber orientation (P-O, AP-O, and N-O) on their tribological behavior. The novelty of this work lies in investigating the effect of temperature on the wear resistance of FGCs with different patterns and fiber orientations. Conventional and FG specimens of long glass fiber-reinforced epoxy composites were fabricated using hand lay-up in the present work, c. The fiber distribution through the FG composite specimens' width was produced in linear, non-linear, and stepwise patterns. Each of these specimens maintained a consistent fiber volume of 38%. Specimen hardness was measured, and a pin-on-disc (POD) tester was prepared to assess the tribological behavior of FGCs and conventional specimens.

2 Materials and methods

2.1 Materials and specimen manufacturing

A hand lay-up technique is utilized to fabricate conventional and functionally graded fiber-reinforced polymers (FRP and FG-FRP) made of unidirectional glass fiber-reinforced epoxy. The matrix material is epoxy (Kemapoxy-150 with a resin-to-hardener ratio of 2:1, provided by Chemical for Modern Building International, CMB, Egypt). This epoxy is a solvent-free, non-pigmented liquid resin with temperature resistance up to 90 °C in wet conditions and 140 °C in dry conditions. It has a pot life of 30 min, reaches full hardness after 7 days, and has a density of 1.12 g/cm^3. It is highly resistant to mechanical stresses and chemical effects. Continuous glass fibers (E6-CR 180), with a diameter of 13 μm and a density of 2.5 g/cm^3, are used as reinforcement, supplied by JUSHI group co. LTD, PRC. Table 1 summarizes the mechanical properties of the materials used in this study. Figure 1 shows a concise flow chart for the manufacturing process of composite plates, raw materials scan (SEM), and specimen preparation for different tests. Finally, the worn surface examination was performed using optical micrographs, SEM images, and XRD analysis.

The X-ray diffraction (XRD) analysis was conducted on conventional FRP and linear FG-FRP patterns to gain insight into their crystalline structures. The XRD results revealed distinct diffraction peaks at specific angles, indicating the presence of crystalline phases within the composite. Figure 2 illustrates the XRD patterns before the wear test, showing a primary peak at 2θ equals 9.9757° and 9.915° for conventional FRP and linear FG-FRP, respectively. The crystallinity values were 65.5% and 60.0% for conventional FRP and linear FG-FRP, respectively, suggesting minimal structural variation due to fiber distribution differences. Generally, lower crystallinity in polymers correlates with reduced mechanical strength and increased wear [35]. Previous studies have shown broad peaks in pure epoxy resins, with diffraction occurring between 5°–80° and maxima near 20°–45°, reflecting the amorphous nature of the cured epoxy network [36, 37]. The absence of additional XRD peaks, as seen in Fig. 2, suggests a uniform distribution of glass fibers within the matrix [38]. Furthermore, no impurities were noticed in the XRD analysis.

Table 1 The mechanical properties of E-glass fiber and epoxy resin

	E (GPa)	G (GPa)	ν	Elongation %
E-glass fiber	82	30.13	0.22	1.8–3.2
Epoxy	3.24	1.1912	0.36	1–8.5

https://doi.org/10.1007/s43452-025-01224-4

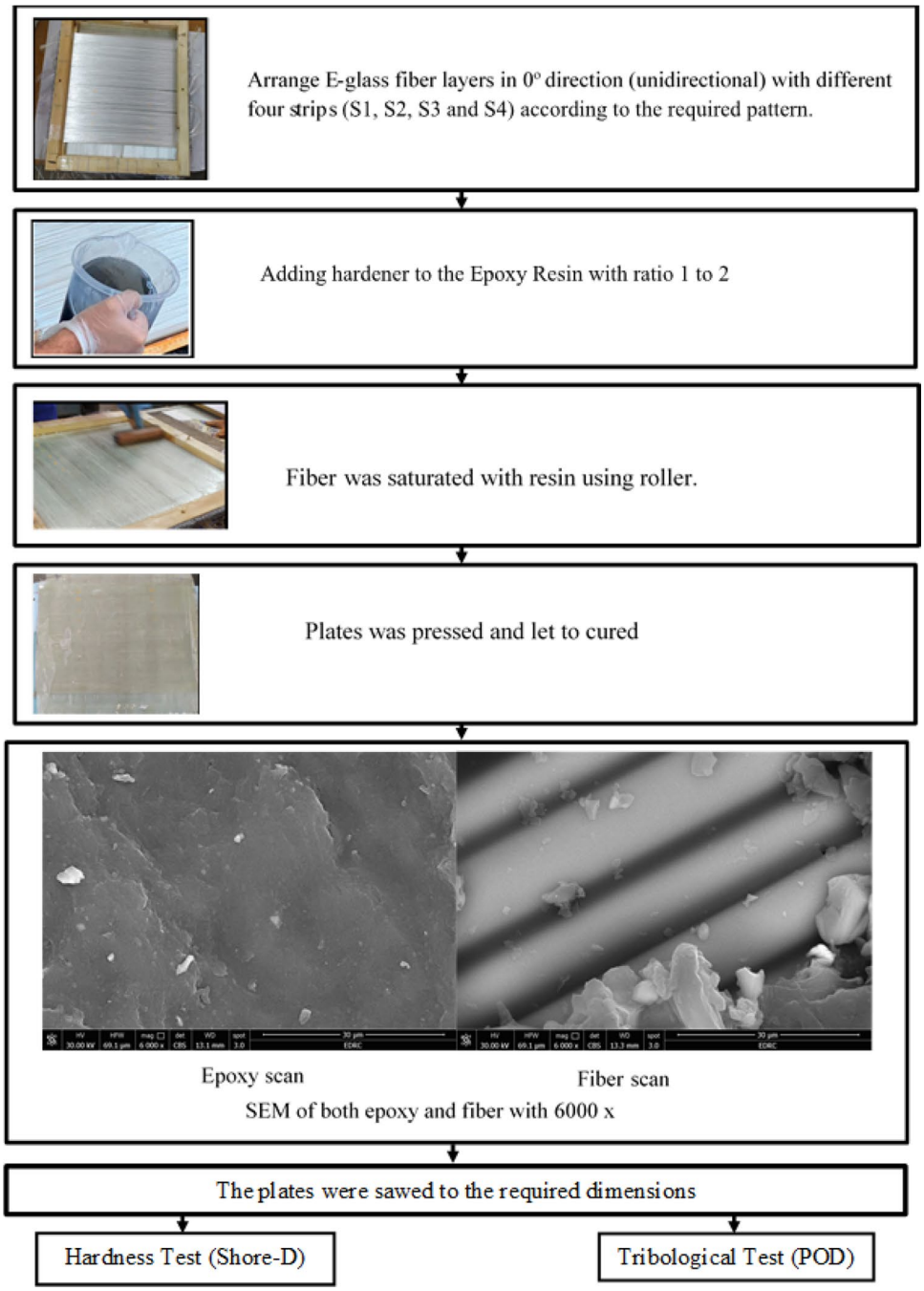


Fig. 1 Flowchart of specimen preparation of the conventional FRP and FG-FRP composites

The conventional FRP and FG-FRP composites are composed of twelve layers, resulting in a total thickness (T) of 12 mm, as shown in Fig. 3. The FG-FRP specimens are created in three different patterns: linear, non-linear, and stepwise. These patterns vary based on the fiber distributions, which depend on the specimen pattern, while the fiber volume fraction is constant through the strip, as listed in Table 2.

Additionally, each layer has an average fiber volume fraction of 38%. A conventional FRP specimen, with a uniform fiber distribution and an average fiber volume fraction of 38%, is used for comparison. Each layer's glass fiber volume fractions (V_f %) are experimentally graded using ignition loss testing, following ASTM D3171 standards [39]. The specimen dimensions are 18 mm width (W), 12 mm thickness (T), and 30 mm length (L), as shown in Fig. 4a. Three different fiber orientations, P-O, AP-O, and N-O, relative to the sliding

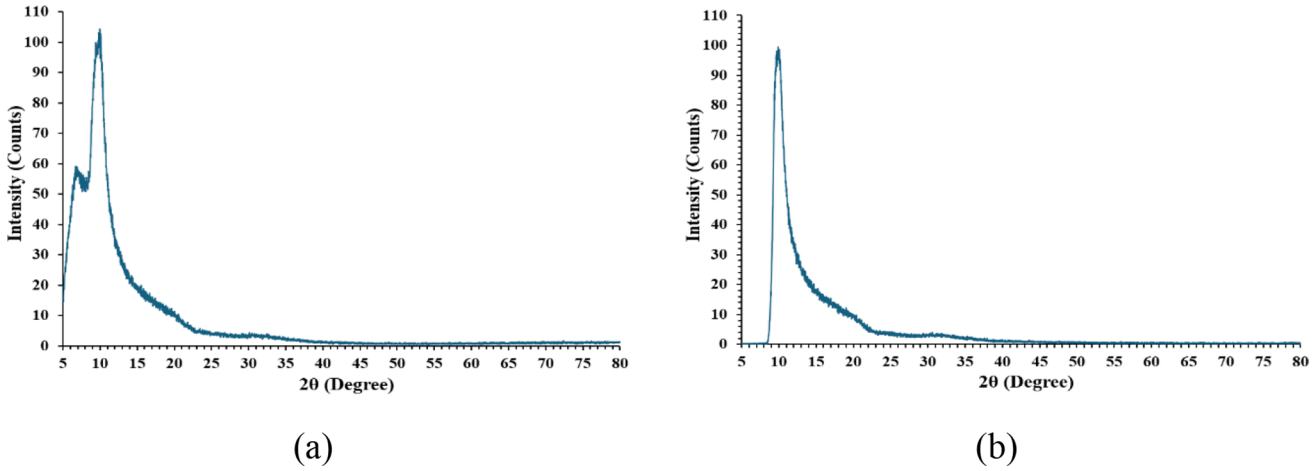


Fig. 2 XRD pattern of **a** conventional FRP and **b** linear FG-FRP

direction of the counter face were studied, as shown in Fig. 4b. Figure 5 illustrates the V_f% through the specimen width for the different patterns.

2.2 Hardness test

Measuring the hardness of conventional and FG composites is a crucial issue. Higher hardness generally indicates better wear resistance. Therefore, hardness tests on both types of composites were performed at room temperature using a Durometer hardness D-scale instrument following ASTM D2240 standards [40]. Figure 6 shows the hardness apparatus, the specimen during testing, and five indentation marks on the specimen after testing.

2.3 Wear test

A pin-on-disk wear test was carried out on both composites according to ASTM F732 standards [41], as depicted in Fig. 7. Before each test, specimens were abraded with 1200-grit SiC abrasive paper and then cleaned with a dry soft brush to ensure uniform surface contact. Tests were conducted under various conditions by varying the load, sliding speed, and sliding distance, considering the effects of fiber orientation relative to the sliding direction.

2.3.1 Sample size effect

The specific wear rate was measured through the wear test to assess the effect of specimen size on wear characteristics by changing the specimen contact area at a constant PV factor, i.e., contact pressure (P) and sliding speed (V), $P = 0.141$ MPa and $V = 1.4$ m/s. The specific wear rate was calculated using Eq. (1) [42].

$$W_s = \frac{\Delta m}{\rho L F_n}, \tag{1}$$

where W_s is specific wear rate (mm^3/N m), Δm is weight loss (g), ρ is density (g/mm^3), F_n is applied load (N), and L is sliding distance (m).

Figure 8 shows the specific wear rate (W_s) of conventional composites (uniform fiber distribution specimens) based on Eq. (1) versus different values of cross-section areas at constant $P \times V$ value. The values of the used areas are 56, 121, 216, and 248 mm^2. The tests were carried out with 180 SiC grit size for 60 s. The figure shows a decrease in the *Ws* values with the increase in the specimen cross-section area to 216 mm^2, which remains nearly constant (the line in Fig. 8). The reversely proportional trend of specific wear rate and direct proportion of the abrasion of the composites with specimen area is in agreement with Wei et al. [43]. So, throughout the rest of the study, the area used was 216

 https://doi.org/10.1007/s43452-025-01224-4

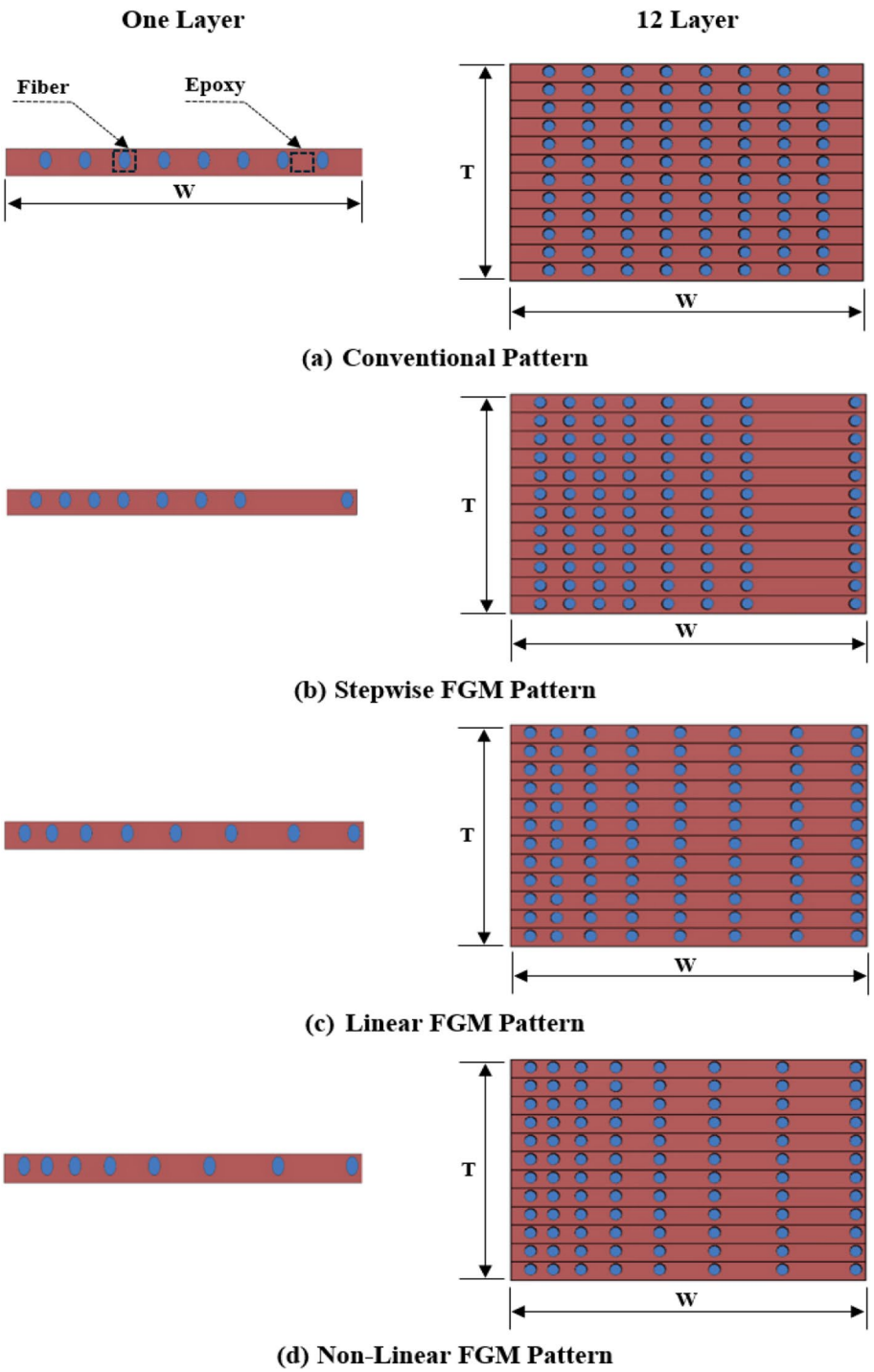


Fig. 3 Fibers distribution in the twelve layers through the thickness of the specimen for the traditional composites and different FGCs patterns

mm^2 (18 mm × 12mm). The prepared composite was machined from the laminate with a 30 mm length. So, dry sliding wear and two-body wear test samples using a tipped cutter, with tribological tests conducted on an 18 mm × 12 mm apparent contact area.

Table 2 The volume fraction and width of the specimen strips

Specimen patterns	Specimen strips	Fiber volume fraction, V_f (%)	Strip width, w_s (mm)
Conventional	S_1–S_4	38	4.5
Linear	S_1	63	2.355
	S_2	39	3.783
	S_3	28	5.211
	S_4	22	6.639
Non-linear	S_1	65	2.151
	S_2	40	3.171
	S_3	29	5.007
	S_4	19	7.659
Stepwise	S_1	49	3
	S_2	49	3
	S_3	36	4
	S_4	18	8

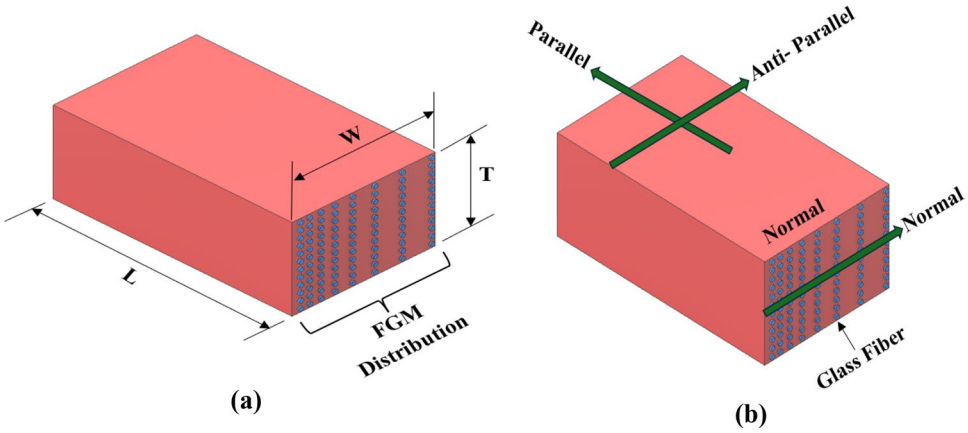


Fig. 4 **a** The specimen dimensions, and **b** fiber directions WRT the direction of the sliding

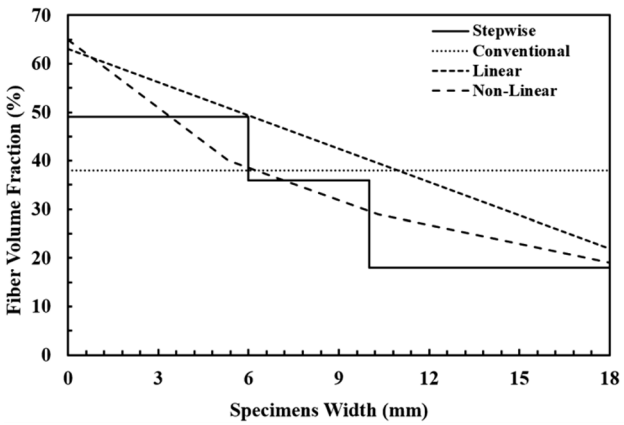


Fig. 5 Fiber distribution through the specimen width for different patterns

 https://doi.org/10.1007/s43452-025-01224-4

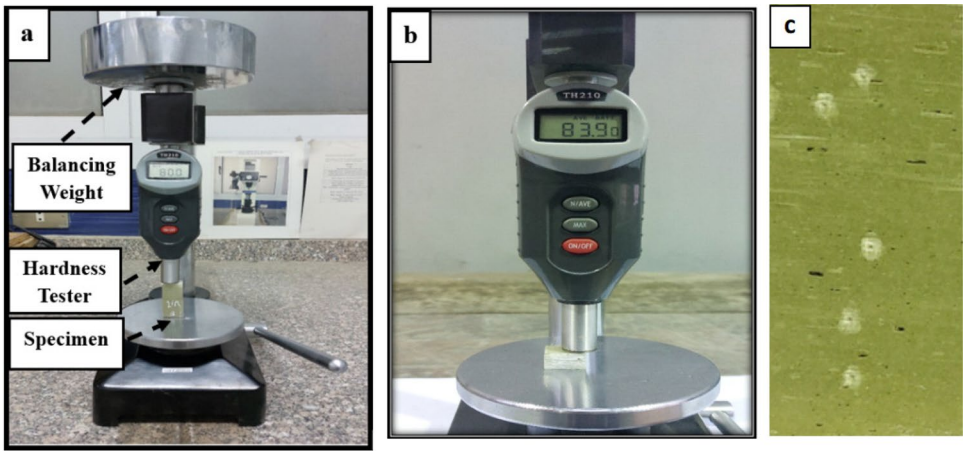


Fig. 6 Hardness measuring: **a** durometer hardness D-scale instrument parts, **b** hardness measuring of linear pattern in (P-O) and (AP-O), and **c** five indentation marks on a specimen

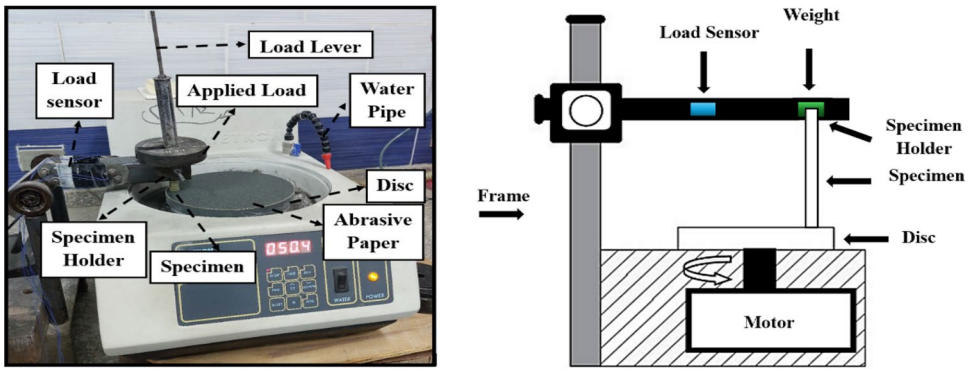


Fig. 7 A pin-on-disk wear test setup

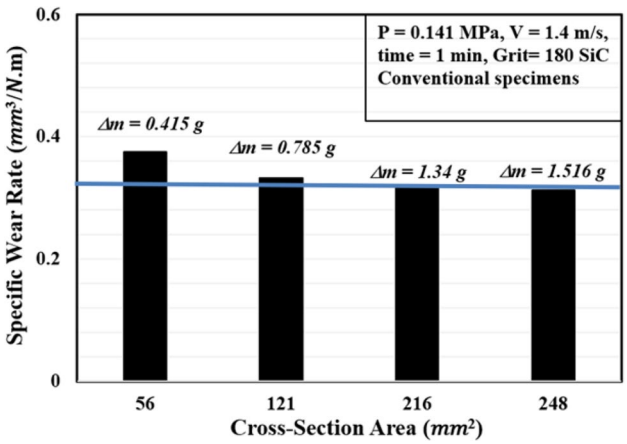


Fig. 8 Specific wear rate variation against specimens' dimensions with constant PV value

2.3.2 Identification of sliding velocity range

An identified study was carried out with varying sliding velocity from 0.2 to 2.5 m/s for one minute to determine a suitable range for sliding speed. An applied load of 30 N was used for the experiments. The abrasive medium for the test was 180 grit SiC abrasive paper. Tests with the above parameters were made on a stepwise pattern of FGCs in the normal orientation to get the effect of sliding speed on the resulting specific wear rate, coefficient of friction, and temperature, as shown in Fig. 9.

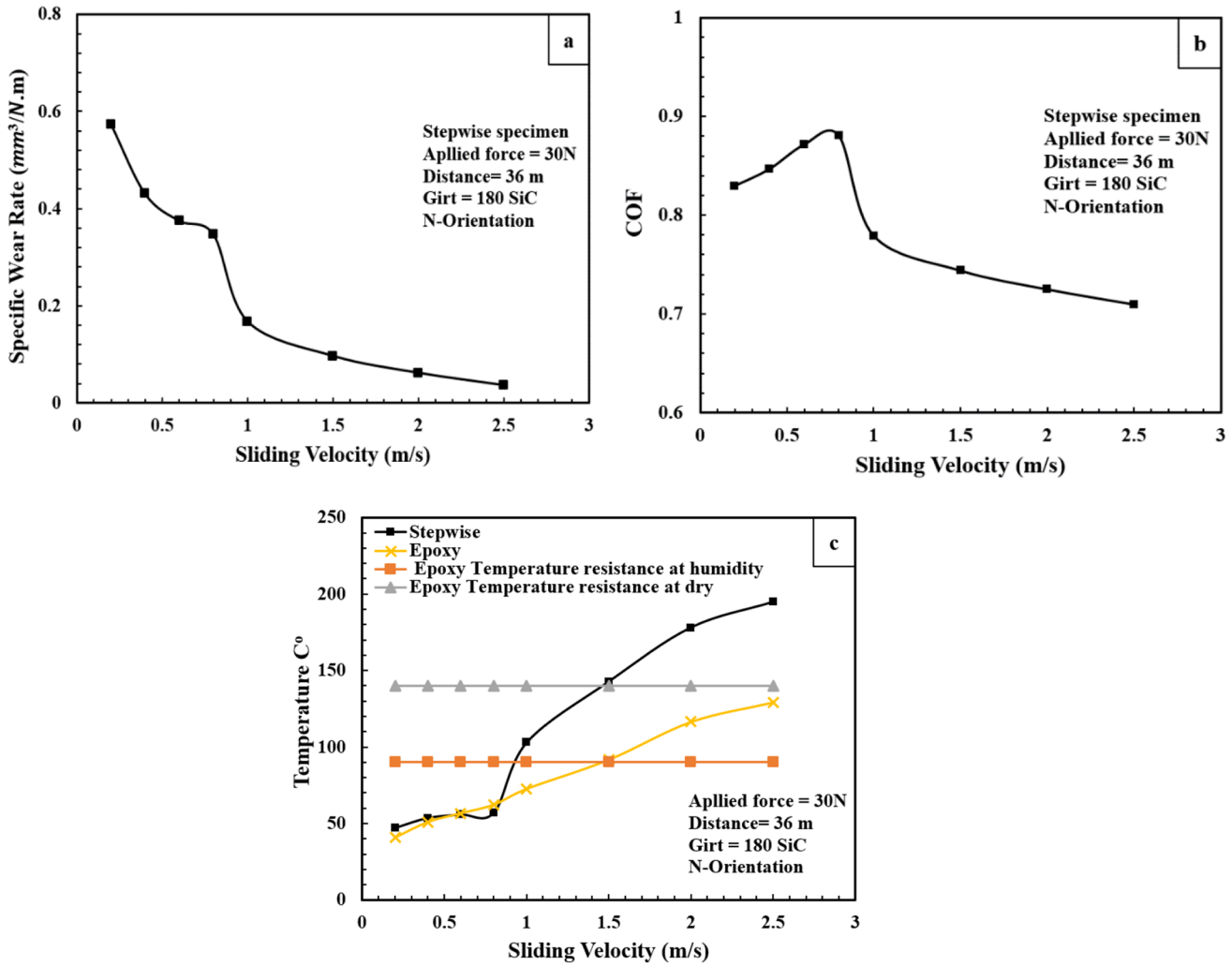


Fig. 9 The effect of sliding velocity on **a** specific wear rate, **b** friction coefficient, and **c** resulting temperature for the FGC stepwise pattern

Figure 9a shows that at a speed less than 0.8 m/s, the degradation of *Ws* decreased, while the slope increased after this stage. Figure 9b shows the relation between the coefficient of friction (COF) and the sliding speed. The speed of 0.8 m/s stands out as a critical point where the slope of the COF curve reverses from ascending to descending. Figure 9c illustrates the variation of temperature values of pure epoxy and the stepwise pattern composite against sliding speed, along with the epoxy temperature resistance under dry and humid conditions. The temperature at sliding speed under 0.8 m/s is increased with a shallow rate, and after this speed value, the rate is raised with high ascending mode. The figure showed that the resulting temperature at a sliding speed higher than 0.8 m/s is higher than the resistance temperature of the epoxy (matrix).

So, during the sliding contact between the specimens and the abrasive SiC paper, the contact layers of the tested composite heat up over time. The epoxy surrounding the fibers softens and smears (at a sliding velocity higher than 0.8 m/s), as shown in Fig. 10. The figure also shows a change in the specimen color due to the friction heating effect at higher speeds. Therefore, a sliding velocity range from 0.2 to 0.8 m/s, in increments of 0.2 m/s, was selected to discuss the two-body abrasive wear behavior of conventional and FG composites.

 https://doi.org/10.1007/s43452-025-01224-4

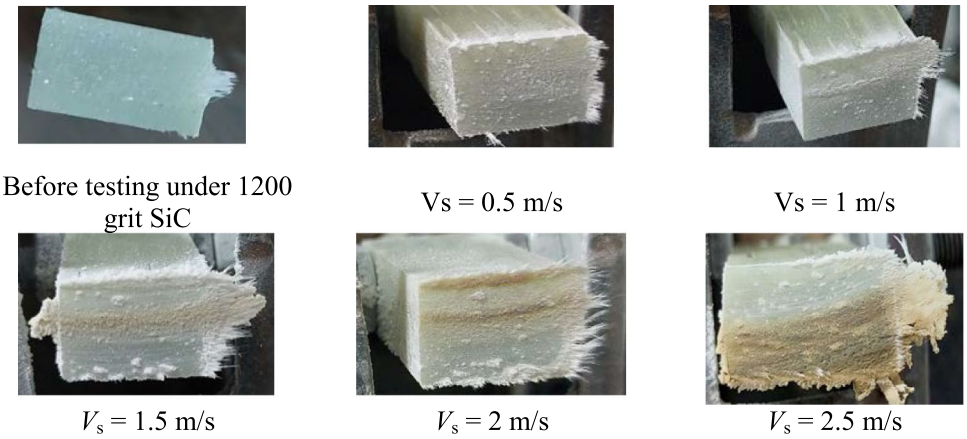


Fig. 10 Photographs showing the effectiveness of V_s on the wear surface of Stepwise specimen in normal orientation (N) under 180 grit SiC

Table 3 The variables examined in the wear test

Parameter	Variation		
	Speed	Load	Time
Applied load (N)	30	10–40 (step 10)	30
Sliding speed (m/s)	0.2–0.8 (step 0.2)	0.6	0.6
Time (min)	1	1	1–4 (step 1)

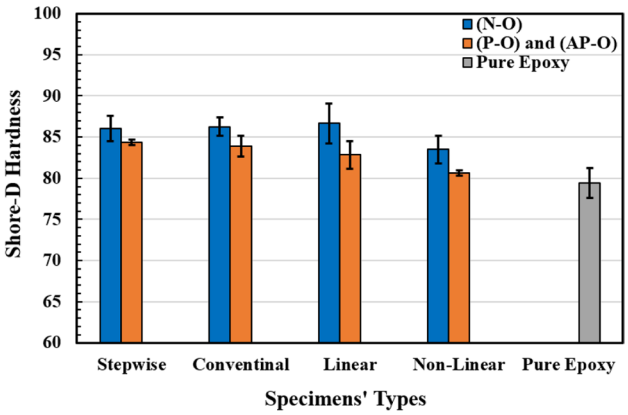


Fig. 11 Variation of hardness

2.3.3 Conditions of wear test experiments

From the above discussion, Table 3 provides details of the experimental parameters. The prepared samples were mounted on a specimen holder. The initial weight of each specimen, including the pin, was measured with an electronic balance accurate to 0.0001 g. Tests were conducted at room temperature (28 °C), and a new specimen was used for each sliding distance. For all experiments, 180-grit SiC abrasive paper was used and glued onto the steel surface of a 200 mm diameter disc.

Reliable data representation was ensured by testing at least three samples to obtain the average abrasive wear loss. The specific wear rate for each operating condition was calculated using Eq. (1). During the tests, the friction force was measured by a load sensor fixed in the middle of the lever. An infrared thermometer was used to measure the maximum interface temperature.

3 Results and discussion

3.1 Hardness of traditional and FG composites

Figure 11 presents the hardness values of traditional and FG composites, considering the impact of fiber orientation alongside the hardness of pure epoxy. Each value was the average of five readings taken from different locations on the specimen, as shown in Fig. 6c. It is clear that the incorporation of continuous glass fibers significantly improves the hardness of pure epoxy. For all types of specimens, hardness values of normal orientation exhibited higher hardness values comparatively compared to those with parallel orientations; this agrees with [44]. This is because the fibers in the orthogonal direction constrain the penetration of the indenter. The hardness values were found to be nearly the same for all patterns (about 86 in the normal direction and 83 in the parallel direction); this may be because all the specimens have the same average V_f%.

In the normal direction, the linear distribution has a slightly improved hardness than the normal one. In comparison, the stepwise pattern shows slightly lower hardness, and the non-linear pattern has the smallest one, with a difference of 3% less than the conventional specimens. This can be referred to as the percentage of higher fiber contents in the contact area, as shown in Fig. 5. In the parallel direction, the stepwise pattern exhibits slightly higher hardness, the linear pattern has slightly lower hardness, and the non-linear pattern shows a 5% decrease. This is also because of the larger area of higher fiber content percentage in the parallel direction, as shown in Fig. 5. The non-linear pattern shows the worst hardness values in both normal and parallel directions. This is because there is a large area with a low fiber percentage in both directions. This gives the impression that it is the worst distribution pattern for fiber.

3.2 Effect of sliding velocity on the wear behavior of composites

The two-body abrasive wear behavior of conventional and FG composites, considering the effects of fiber orientations, as shown in Figs. 12, 13 and 14. The effect of the sliding velocity has been noted in three resulting phenomena (*Ws*, COF, and temperature). A varying sliding velocity from 0.2 to 0.8 m/s, in increments of 0.2 m/s, was selected for one minute. Additionally, an applied load of 30 N was used for the experiments. The abrasive medium for the test was 180 grit SIC abrasive paper.

3.2.1 Specific wear rate

Figure 12 shows the specific wear rate of conventional and FG composites in three fiber orientations as a function of sliding speed. The *Ws* in the normal direction is lower than that in the parallel and anti-parallel directions due to the orientation of the fibers; this agrees with [24, 25]. For the normal direction (Fig. 12c), the *Ws* decreased with the speed increase for all patterns. The linear pattern outperformed the conventional one, while the stepwise pattern performed worse, and the non-linear pattern performed the worst.

Additionally, the slope of *Ws* for stepwise specimens is steeper than for conventional ones, while the linear specimens exhibit the shallowest slope. The parallel direction (Fig. 12b) shows a reverse order between stepwise and linear patterns, while the non-linear pattern keeps the worst performance. The trends of all the patterns are ascending. In the anti-parallel friction test (Fig. 12a), the conventional distribution has the highest value, while the stepwise distribution has the lowest value. The trend of *Ws* with sliding velocity is ascending for patterns, except for the stepwise pattern, which is descending. These results are consistent with the hardness measurements (Fig. 11) and the fiber distribution (Fig. 5).

 https://doi.org/10.1007/s43452-025-01224-4

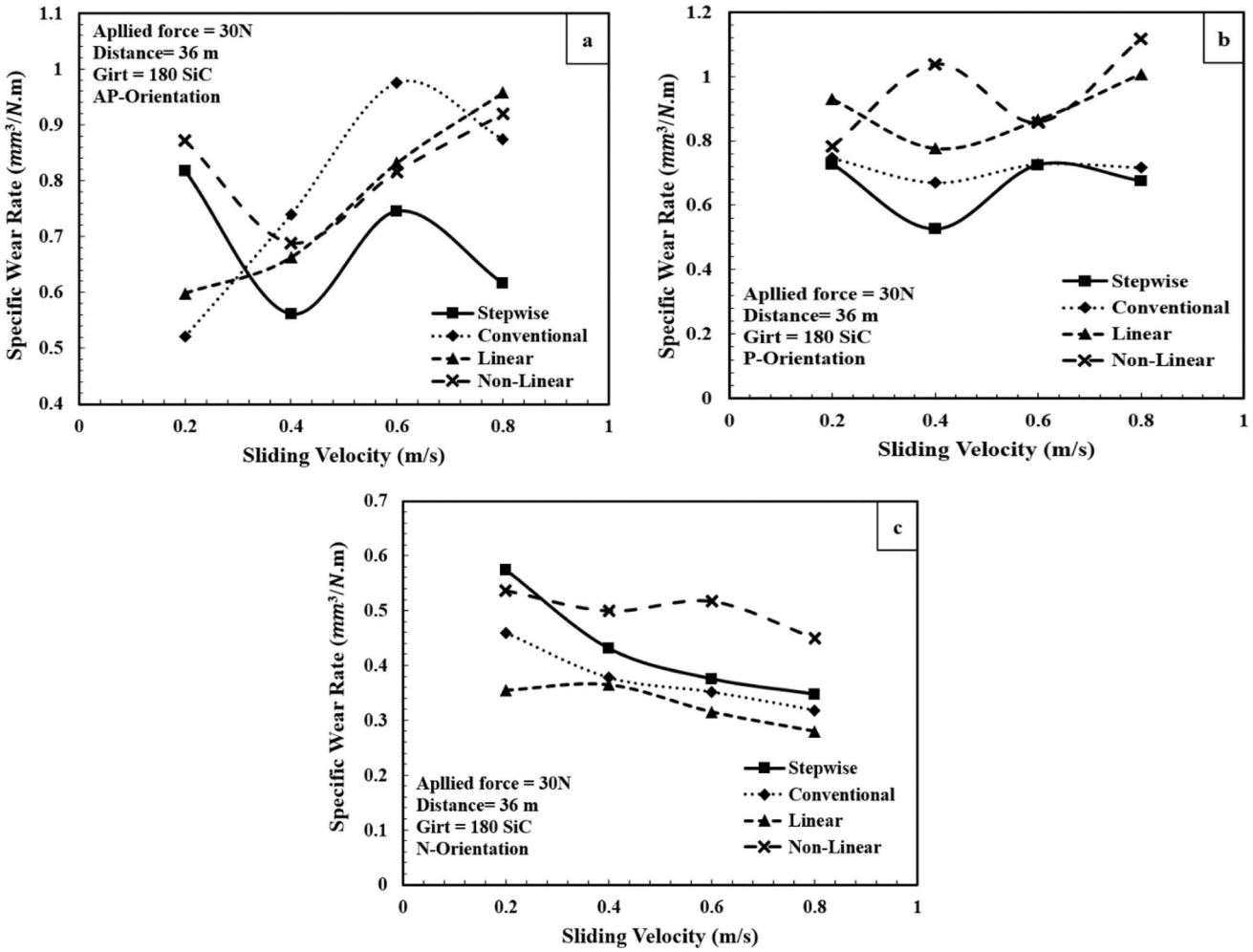


Fig. 12 Specific wear rate of traditional and FG composites as a function of sliding speed: **a** anti-parallel, **b** parallel, and **c** normal

3.2.2 Coefficient of friction

Figure 13 illustrates the trend and variation of COF values of traditional and FG composites against sliding velocities. It is observed from the figure that there is a proportional relation between COF values and sliding velocity for all three fiber orientations and all the fiber distribution patterns. The COF of N-O, Fig. 13c, is higher than that of other fiber orientations, Fig. 13a, b. In the case of normal orientation, the linear pattern exhibits the lowest COF values for all values of the sliding velocity, as shown in Fig. 13c. However, the stepwise and non-linear patterns demonstrate higher COF values than traditional composite in N-O. Conversely, the stepwise pattern, in the cases of AP-O and P-O, exhibits the lowest COF values for all values of the sliding velocity compared to conventional composite and other distributions of FG composites, as shown in Fig. 13a, b.

3.2.3 Temperature

Figure 14 illustrates the trend and variation of maximum interface temperatures of conventional and FG composites measured during the wear test at different sliding velocities in all three orientations. It is observed

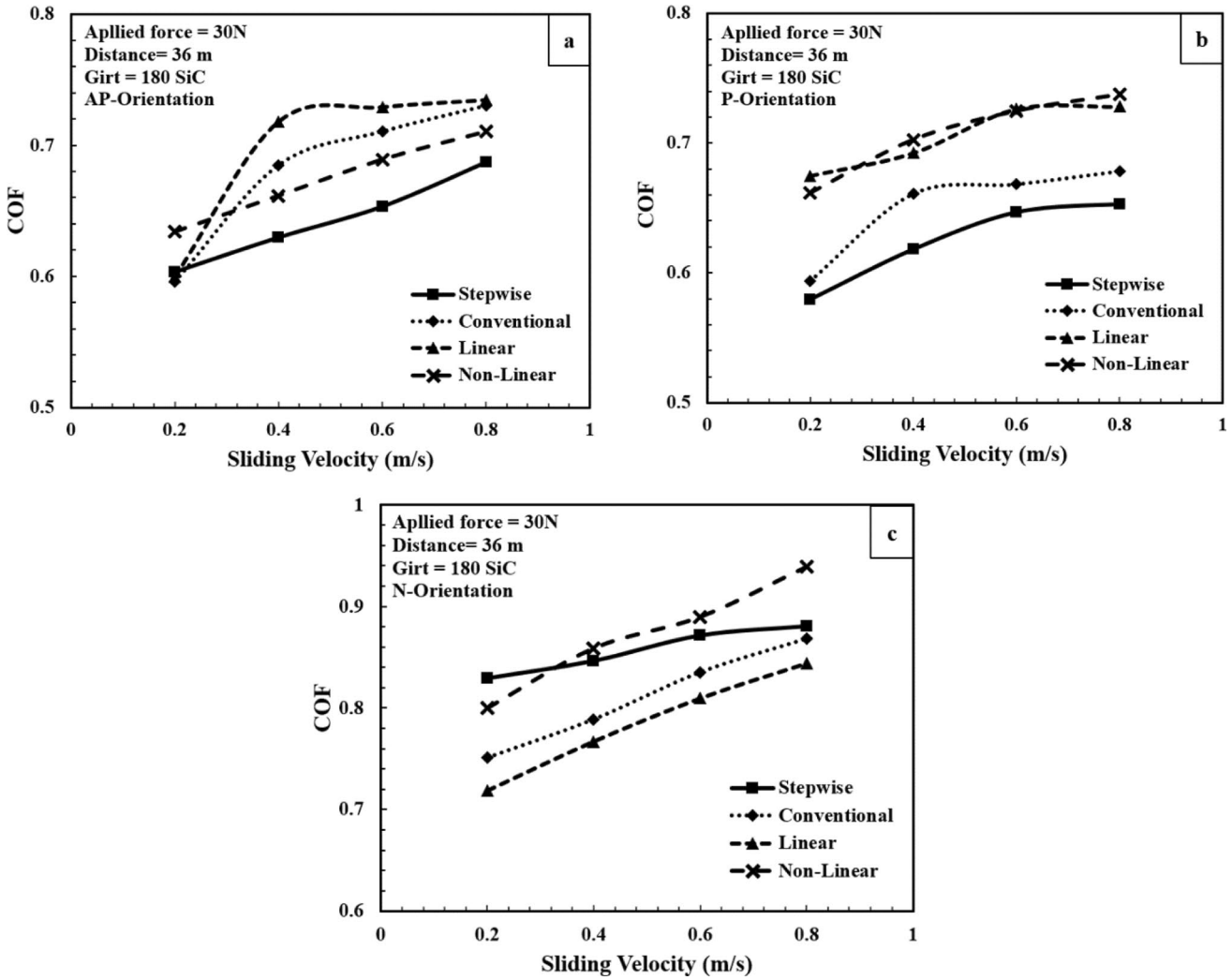


Fig. 13 Coefficient of friction versus sliding velocity for conventional and FG composites under different orientations: **a** anti-parallel, **b** parallel, and **c** normal

from the figure that there is a proportional relation between the interface temperature and the sliding velocity. Because of the high COF of conventional and FG composites in N-O, Fig. 14c, higher interface temperatures were produced than conventional and FG composites in P-O and AP-O, Fig. 14a, b. The temperature for all friction orientation and fiber patterns is directly proportional to the sliding speed.

A change in the escalation slope of the temperature of all fiber patterns and friction directions at 0.4 m/s sliding velocity can be noted in Fig. 14. The ascending rate is decreased after this point, i.e., 0.4 m/s sliding velocity. The shadow of this notice was reflected in most of Fig. 12 in the change in the descending rate of *Ws* (Fig. 12c) or changed the descending of it into ascending (Fig. 12a, b). Also, the same thing happened in Fig. 13a–c in the change of ascending rate of COF for all specimens.

3.3 Applied load effects

Applied load effects on the two-body abrasive wear behavior of conventional and FG composites have been studied and presented in Figs. 15, 16 and 17 for the studied patterns and orientations. The varying sliding

 https://doi.org/10.1007/s43452-025-01224-4

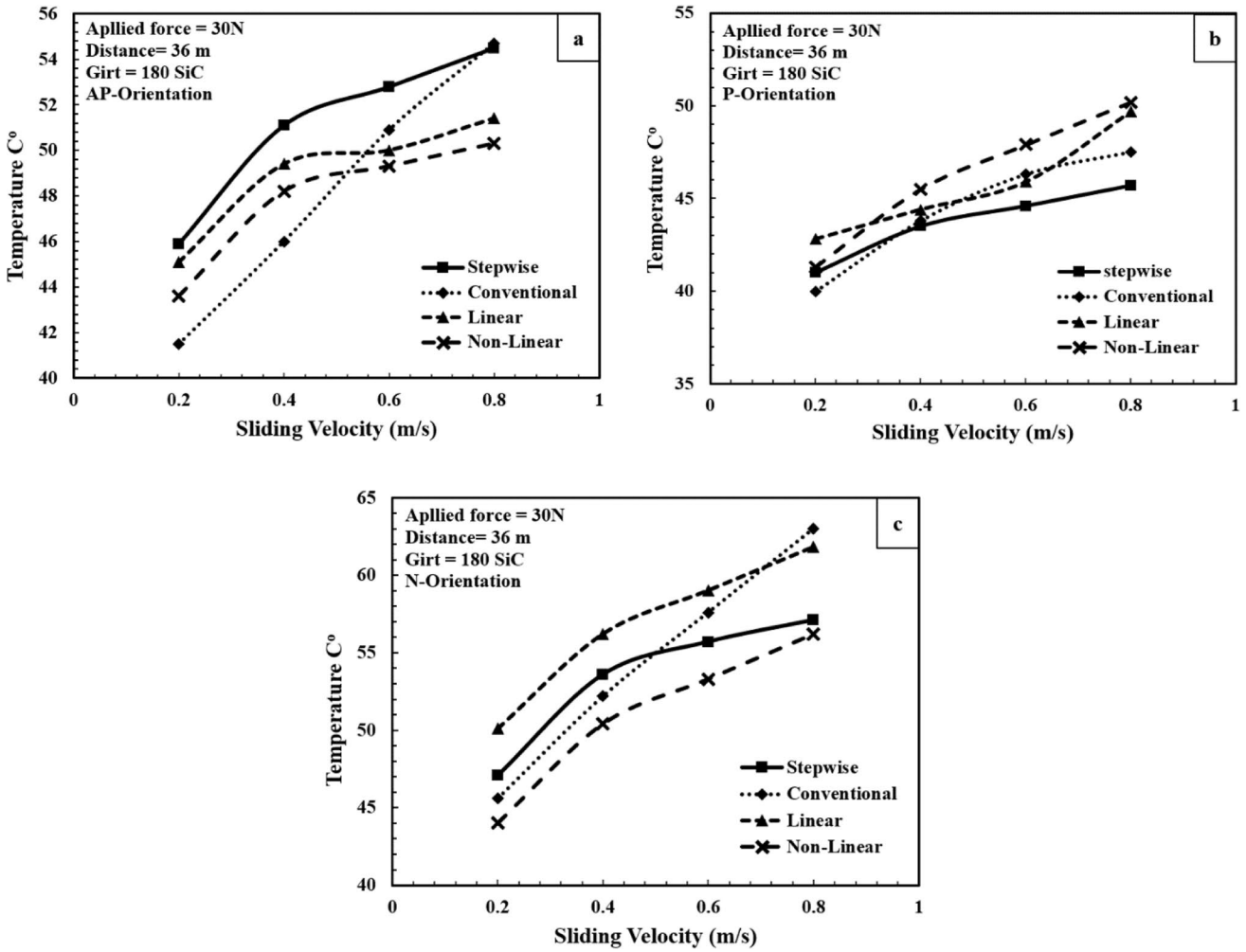


Fig. 14 Temperature versus sliding velocity for conventional and FG composites under different orientations: **a** anti-parallel, **b** parallel, and **c** normal

load of 10 N up to 40 N in steps of 10 N has been selected for an abrading distance of 36 m, sliding velocity of 0.6 m/s, and abrasion media of 180 Grit SiC abrasive paper.

3.3.1 Specific wear rate

Figure 15 illustrates the trend and variation of the *Ws* against the applied load. It is observed from the figure that there is a linear decrease in specific wear rate with the increase in abrasion load in (AP-O and N-O), Fig. 15a–c; this agrees with [44]. However, the specific wear rate of linear and non-linear patterns relatively increased with the rise in applied load in P-O, Fig. 15b. The lowest specific wear rate of traditional and FG composites is in the N-O direction, Fig. 15c, compared to P-O and AP-O directions, Fig. 15a, b. Figure 15 indicates that the linear pattern exhibits the highest resistance to abrasive wear as the abrasion pressure increases, compared to other patterns in N–O. However, the stepwise and non-linear patterns demonstrate lower abrasive wear resistance than the conventional ones in N. Conversely, the stepwise pattern exhibits the highest resistance to abrasive wear as the abrasion pressure increases, compared to the conventional ones and other patterns in AP-O and P-O.

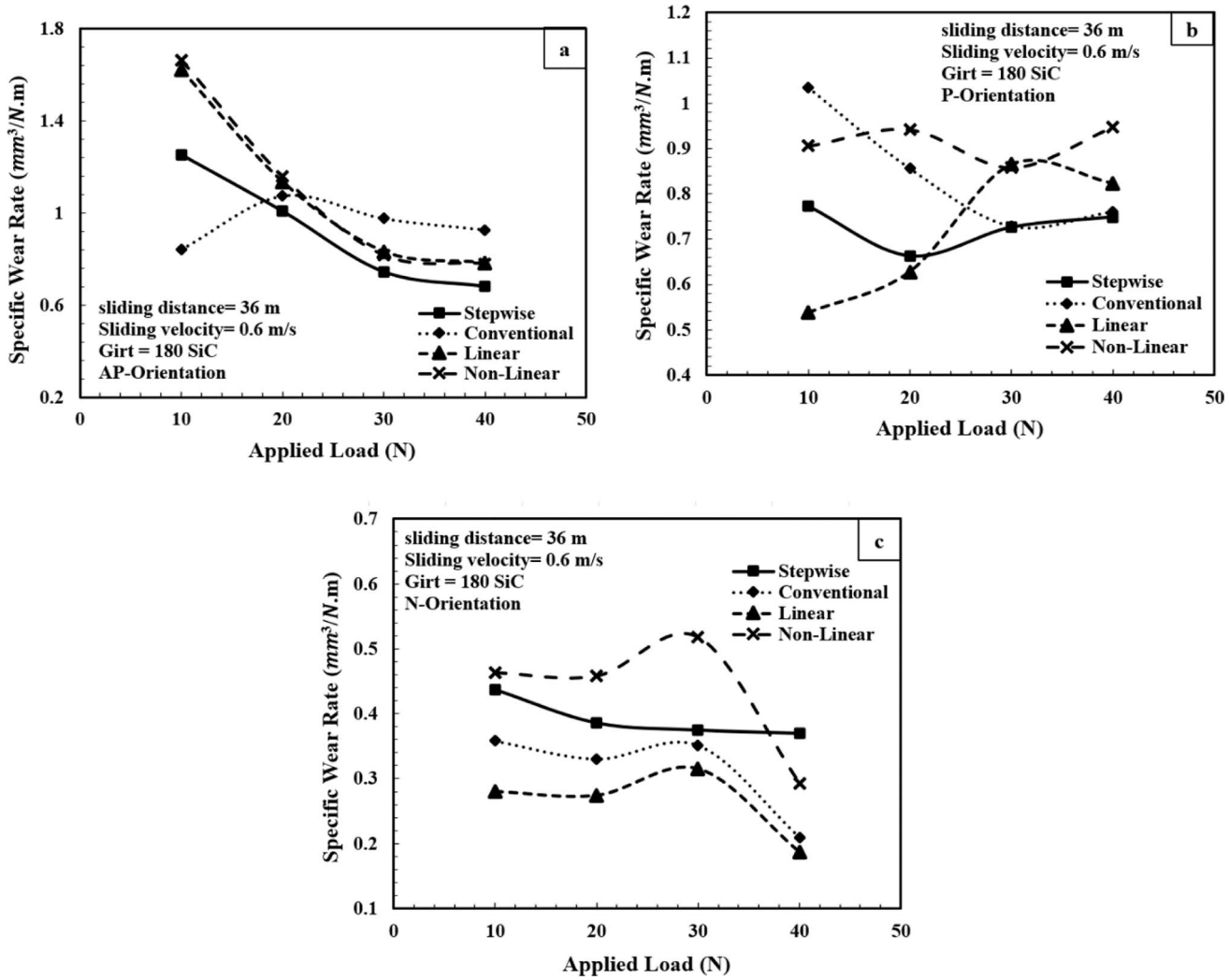


Fig. 15 Specific wear rate versus applied loads for conventional and FG composites under different orientations: **a** anti-parallel, **b** parallel, and **c** normal

3.3.2 Coefficient of friction

Figure 16 illustrates the trend and variation of the COF of conventional and FG composites against the applied load (10–40 N). It is observed from Fig. 16c that an increase in COF values is observed with the increase in abrasion pressure in N-O. In contrast, in AP-O and P-O, the COF values decrease with increased abrasion pressure, as shown in Fig. 16a, b.The highest coefficient of friction (COF) of conventional and FG composites in N-O, as shown in Fig. 16c, compared to conventional and FG composites in P-O and AP-O, as shown in Fig. 16a, b. Figure 16 indicates that the linear pattern exhibits the lowest COF values as the applied loads increase, compared to other patterns in N-O. However, the stepwise and non-linear patterns demonstrate higher COF values than the conventional ones in N-O. Conversely, the stepwise pattern exhibits the lowest COF values as the applied loads increase, compared to the conventional ones and other patterns in AP-O and P-O.

3.3.3 Temperature

Figure 17 illustrates the trend and variation of maximum interface temperatures of conventional and FG composites that were measured during the wear test at different applied loads in all three orientations. It is observed from

 https://doi.org/10.1007/s43452-025-01224-4

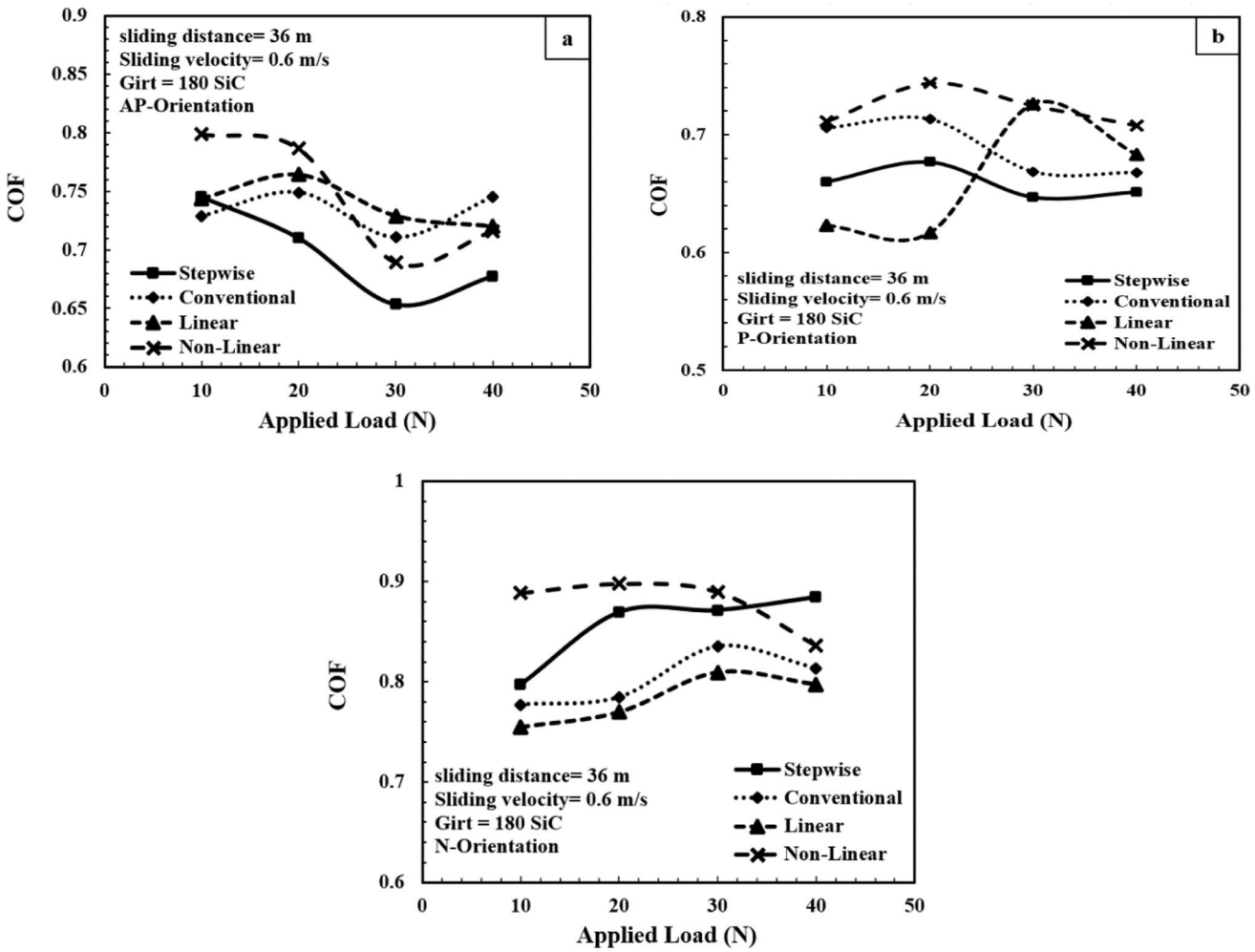


Fig. 16 Coefficient of friction versus applied loads for conventional and FG composites under different orientations: **a** anti-parallel, **b** parallel, and **c** normal

the figure that the interface temperature increases with the increase in applied loads. Because of the high COF of conventional and FG composites (in N-O), as shown in Fig. 17, a higher interface temperature was produced than conventional and FG composites in P-O and AP-O; this agrees with [24]. When comparing Fig. 17 with Fig. 14, It was found that the influence of sliding velocity on the maximum interface temperature of conventional and FG composites against the disc is higher than that of applied force on the maximum interface temperature in all three orientations.

A change in the escalation slope of the temperature of all fiber patterns and friction directions at applied force 30 N is noted in Fig. 17. The ascending rate decreased dramatically after this point for all studied cases. The shadow of the note is reflected in most of Fig. 15, either in the change in the descending rate of *Ws* (Fig. 15a, c) or in the reversal from descending to ascending (Fig. 15b). Also, the same thing happened in Fig. 16a–c in the change of descending COF for all specimens into ascending.

3.4 Effect of sliding distance

Variations of specific wear rate and coefficient of friction of conventional and FG composites in the normal orientation were analyzed concerning variation in the sliding distance. At the same time, all other parameters were kept constant in Fig. 18. A varying sliding distance from 36 to 144 m, in increments of 36 m (corresponding to

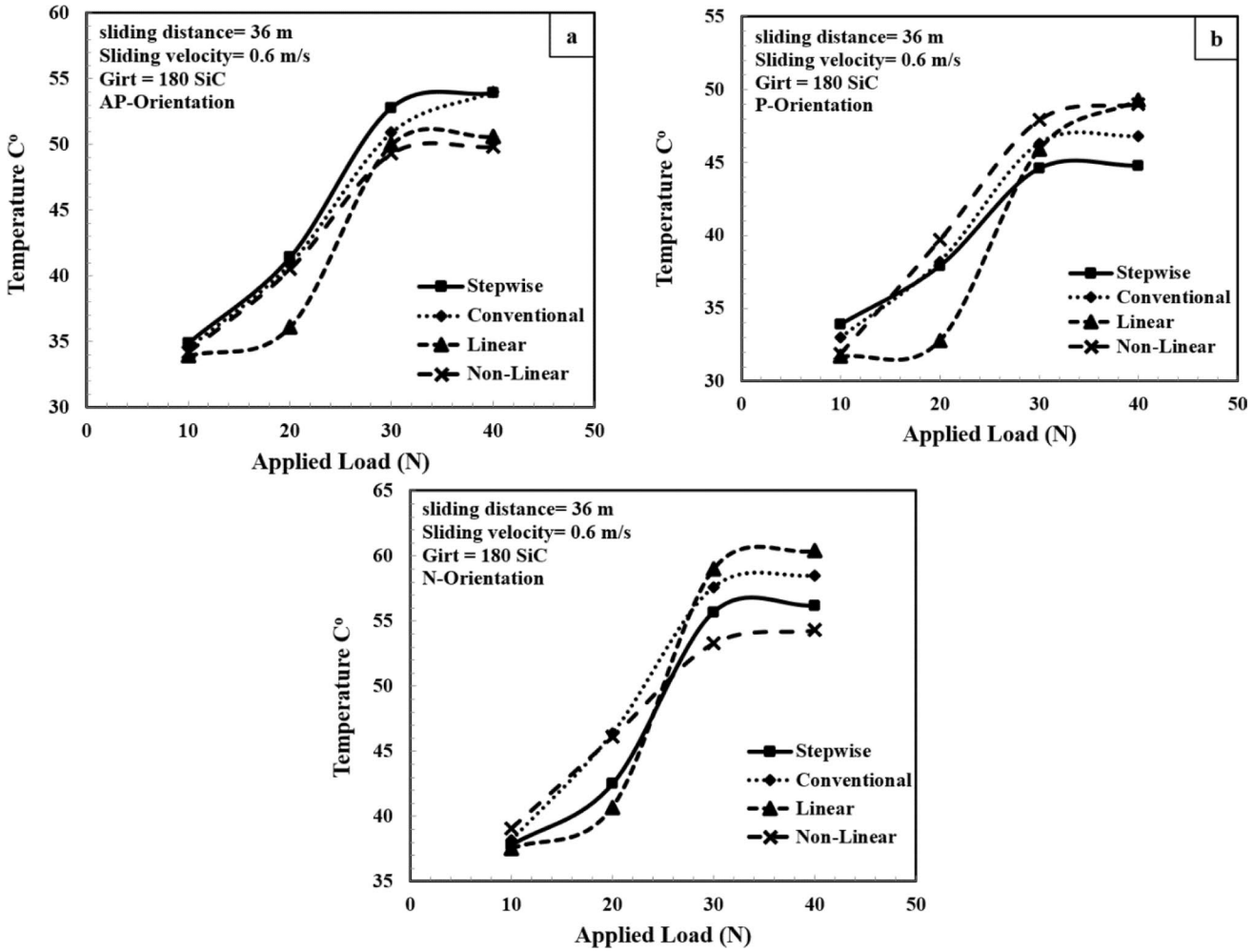


Fig. 17 Temperature versus applied loads for conventional and FG composites under different orientations: **a** anti-parallel, **b** parallel, and **c** normal

sliding time 1–4 min and step 1 min), was selected to achieve the experiments. Additionally, an applied load of 30 N and a speed of 0.6 m/s were used for the experiments. The abrasive medium for the test was 180 grit SIC abrasive paper. Figure 18 shows that the specific wear rate decreases with sliding distance. However, the coefficient of friction (COF) and temperature were increased with sliding distance. The linear pattern exhibits the highest resistance to abrasive wear as the sliding distance increases compared to other patterns. However, the stepwise and non-linear patterns demonstrate lower abrasive wear resistance than the conventional ones. This difference is attributed to the non-linear and stepwise distributions, which often involve a more random or varied arrangement of fibers than the conventional and linear distributions in normal orientation (N-O).

3.5 Surface morphology

In this section, optical microscope and SEM images and XRD analyses are presented and discussed to enhance comprehension of the tribological behavior of the present functionally graded materials. Many researchers have conducted surface morphology of worn surfaces using optical microscope images only, obtaining acceptable findings in determining wear characteristics [45, 46]. Figure 19 illustrates an optical micrograph for the obtained contact surfaces after resin removal, revealing partially exposed fibers and dark abrasion grooves due to depth variations. Over time, these exposed fibers undergo pulverization as a result of wear. The micrograph in Fig. 19a

 https://doi.org/10.1007/s43452-025-01224-4

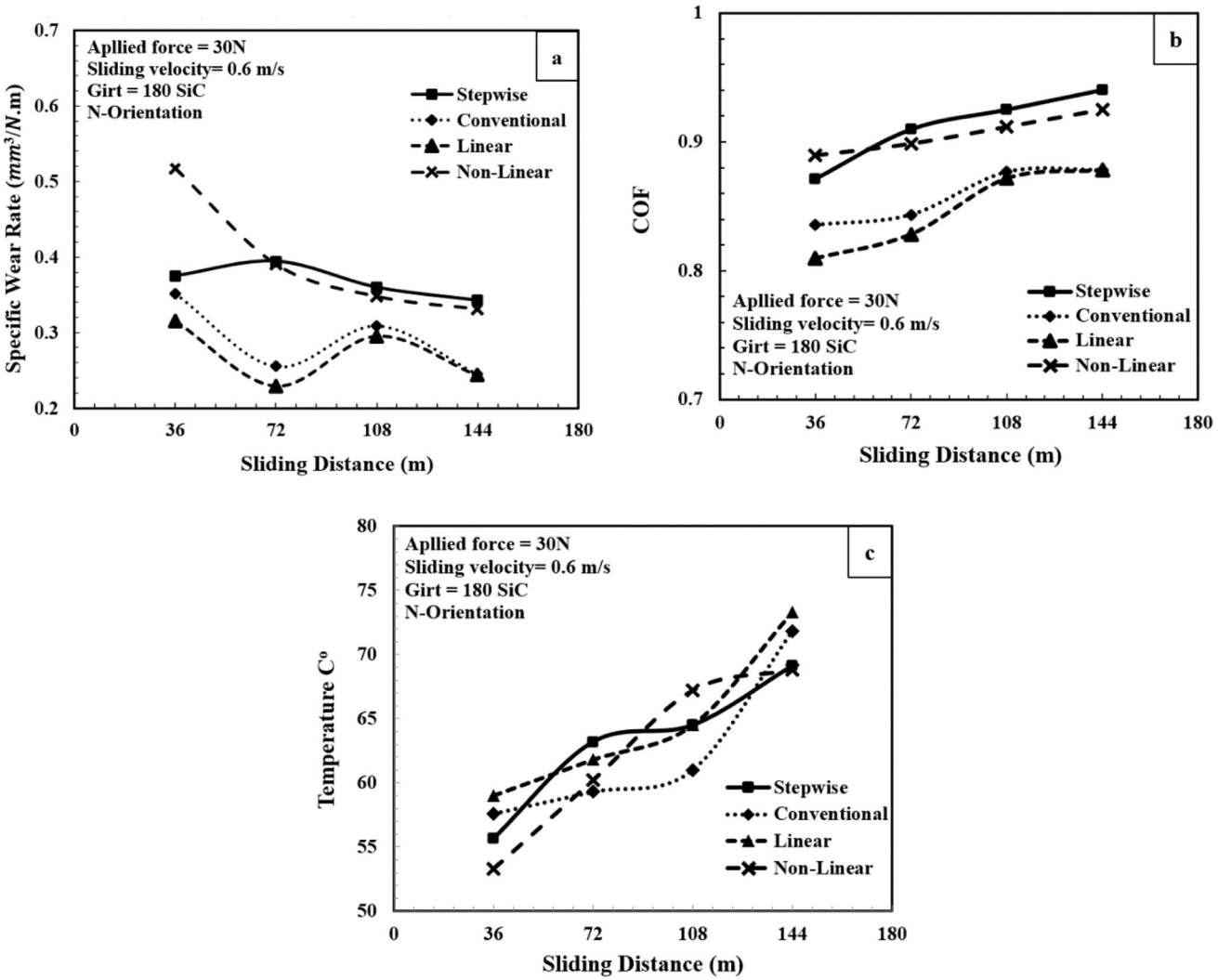


Fig. 18 Abrasive wear response of conventional and FG composites in two body wear modes against sliding distance: **a** specific wear rate, **b** COF, and **c** temperature

highlights craters formed by resin detachment following surface cracking. Similar wear mechanisms, including resin cracking and fiber exposure, have been previously reported for fiber-reinforced composites based on SEM images [47, 48]. These matched the earlier opinion of Zheng et al. [49], which was based on the results of both optical microscope and SEM images. They stated that resin removal was the initial wear mechanism, where surface cracks in the resin trigger the wear process. These cracks developed due to shear stress induced by the slip component, leading to resin detachment and exposing the subsurface composite material.

It is clear that fiber orientation significantly influences the wear characteristics of the present composites. This may be elucidated through a suggested mechanism of the wear for the present composites in all three orientations, as depicted in Fig. 19. In this proposed mechanism, it is recommended that the damage within the region of the fibers varies depending on the orientation. Two damages may occur in parallel orientation (Fig. 19a): fiber breakage or bending along the sliding direction. The adhesion properties between the fibers and the matrix primarily control this. If the adhesion properties are sufficiently robust to avoid fiber twisting or debonding, the fibers may experience tearing and breakage. However, debonding, bending, and eventual detachment of the fibers may occur if the side force exceeds the interfacial adhesion strength. This scenario is likely for anti-parallel orientation, as shown in Fig. 19b. Conversely, in the normal orientation, where the fiber ends are exposed to the counter face

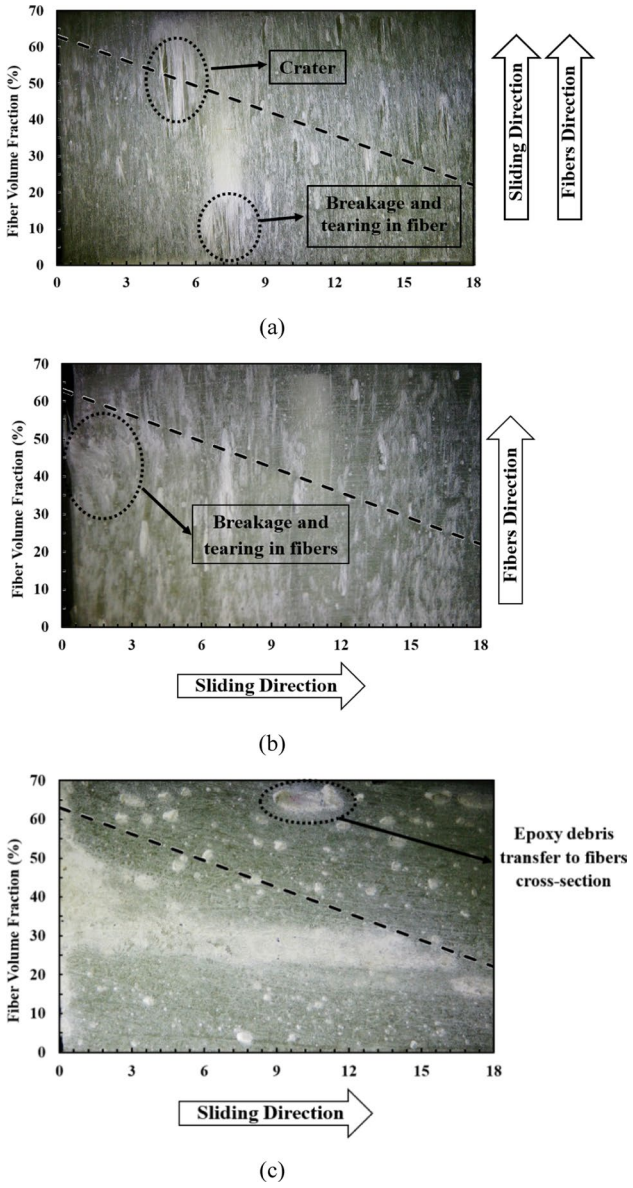


Fig. 19 Suggested wear mechanism of a linear pattern of FGCs at 30 N applied load and 0.6 m/s sliding velocity: **a** parallel orientation, **b** anti-parallel orientation, and **c** normal orientation

(Fig. 19c), detachment is unlikely due to the fibers being fixed within the matrix. On the other hand, cracks are formed near the fibers, normal to the sliding direction, as shown in Fig. 19c. This can be further clarified by observing the worn surface of the composite.

Figure 20 presents optical micrographs of FGC and conventional composite specimens after undergoing wear tests under a normal load of 30 N and a sliding speed of 0.6 m/s. Peeled-off or broken matrix and fiber fragments appear as wear debris on the surface. Before this, various damage mechanisms occurred, including fiber pull-out, matrix-fiber debonding, and matrix loss. As wear progresses, increased load on the fibers due to matrix deterioration leads to fiber thinning and eventual breakage, as depicted in Fig. 20. The wear process begins with a temperature rise caused by friction at the contact surface between the composite and its counterpart. Due to the brittle nature of epoxy, this temperature increase initially causes matrix softening and cracking. Microcracks form and gradually expand in different directions, leading to the development of advanced crack zones. As these cracks propagate deeper into the composite, they weaken the fiber-matrix interfacial bonds, causing separation and further accelerating material degradation. The wear performance of stepwise patterns is influenced by normal load and sliding velocity, as shown in Figs. 21 and 22. With increasing sliding velocity, the roughness of

https://doi.org/10.1007/s43452-025-01224-4

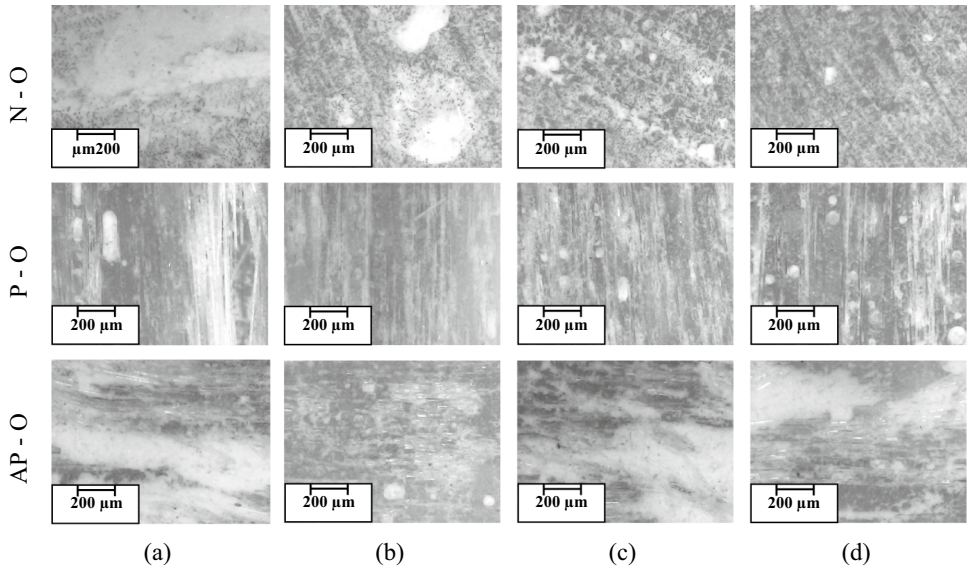


Fig. 20 Investigation of the worn surfaces of specimens under an applied load of 30 N and sliding velocity of 0.6 m/s in all three orientations for **a** conventional, **b** stepwise, **c** non-linear, **d** linear

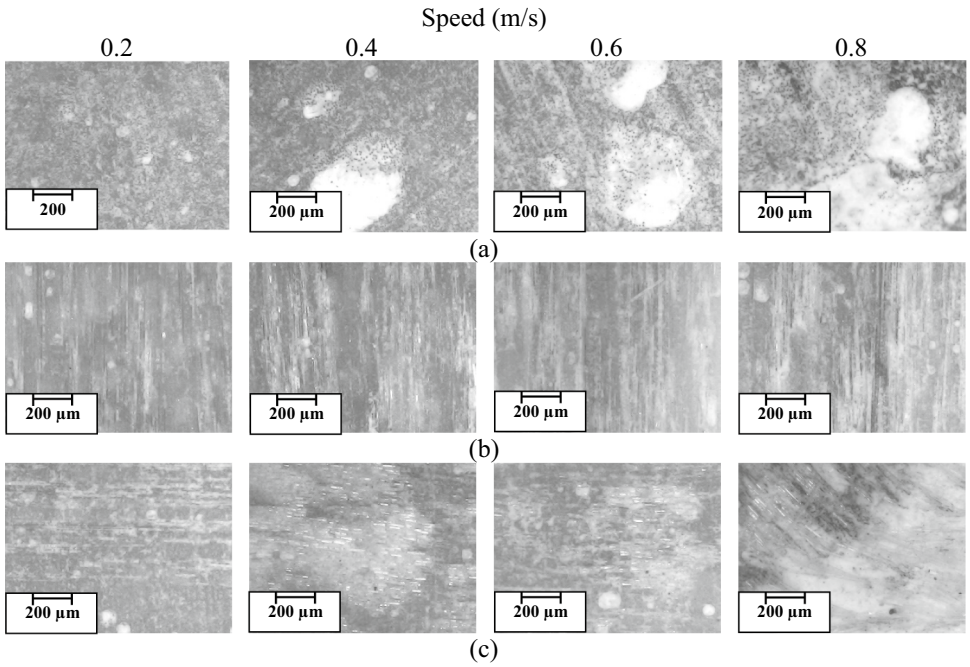


Fig. 21 Investigation of the worn surfaces of stepwise specimens under an applied load of 30 N at various sliding velocities for **a** N–O, **b** P-O, and **c** AP-O

the worn surface also increases due to higher heat generation and surface fatigue, which weakens the specimen. Large craters form as matrix material is lost, while grooves appear due to fiber separation under higher loads and sliding velocities, leading to a rougher wear surface. This is clear from the SEM images Figs. 24 and 25.

SEM images, Figs. 23, 24 and 25, illustrate the abraded surfaces of fiberglass-epoxy composites at different orientations. Fiber debonding was observed in the linear pattern at N-O under 30N load and 0.6 m/s sliding velocity (Fig. 23) due to high thermo-mechanical loading, accelerating material removal, and weakening fiber-matrix adhesion. Despite this, fiber ends still bear some load without signs of pull-out. Micro-cracks appear due to high side forces, indicating strong wear resistance at the rubbing zone. This suggests that under severe conditions, the dominant wear mechanism in N-O is micro-cracking, supporting the proposed wear mechanism (Fig. 19c).

Figure 24 demonstrates significant fiber-matrix compatibility, as evidenced by the uneven surface wear. Fiber debonding was observed when fiberglass-epoxy composites were tested in P-O under a 40N load and

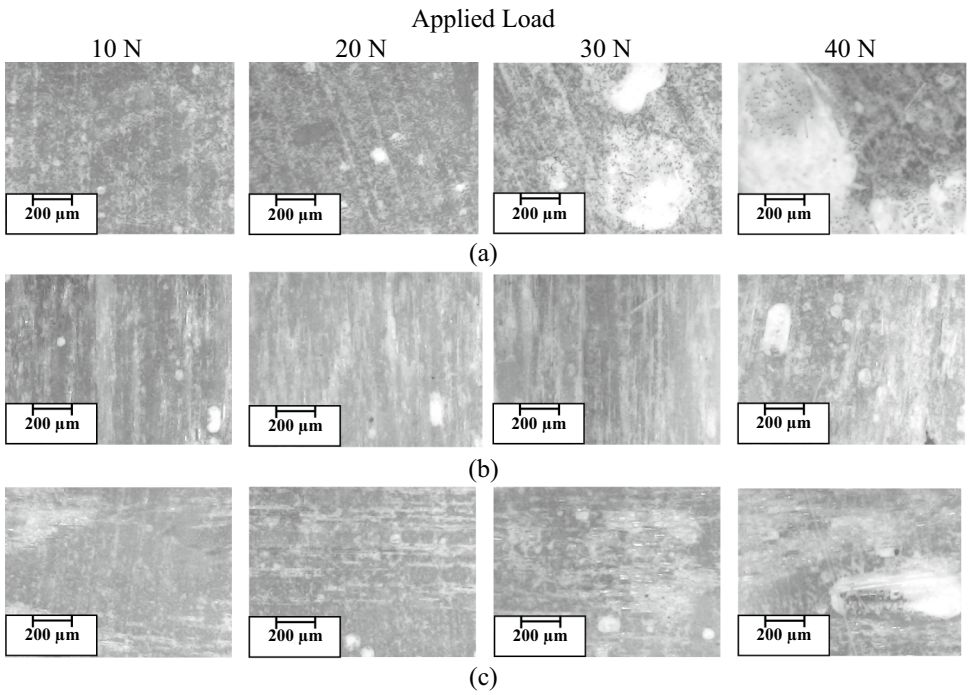


Fig. 22 Investigation of the worn surfaces of stepwise specimens under various applied loads at a sliding velocity of 0.6 m/s for **a** N–O, **b** P-O, and **c** AP-O

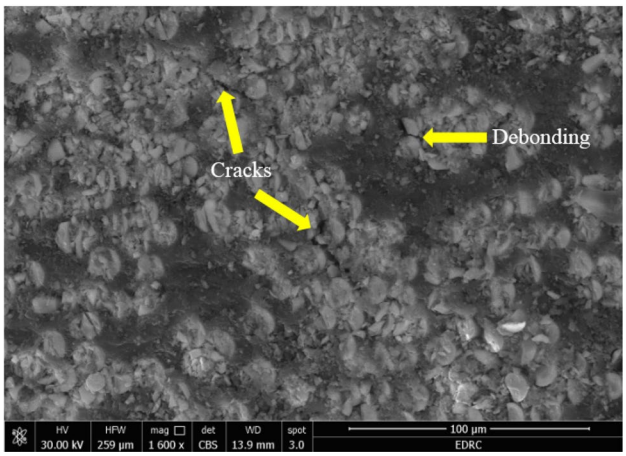


Fig. 23 SEM images of the abraded surfaces of the FRP composite (linear pattern) in N–O at 30 N applied load and 0.6 m/s sliding velocity for 144 m sliding distance

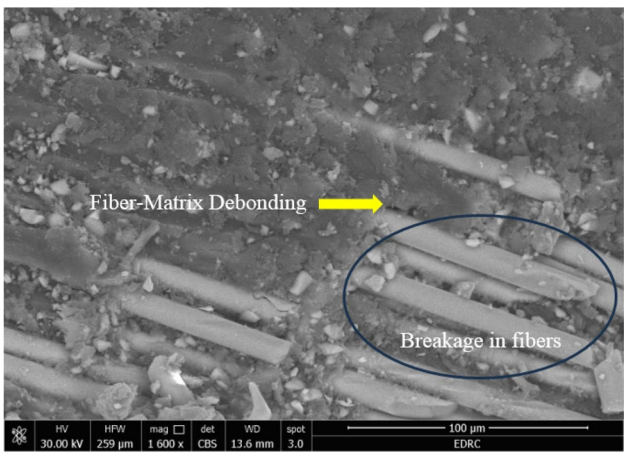


Fig. 24 SEM images of the abraded surfaces of the FRP composite (stepwise pattern) in P-O at 40 N applied load and 0.6 m/s sliding velocity for 36 m sliding distance

https://doi.org/10.1007/s43452-025-01224-4

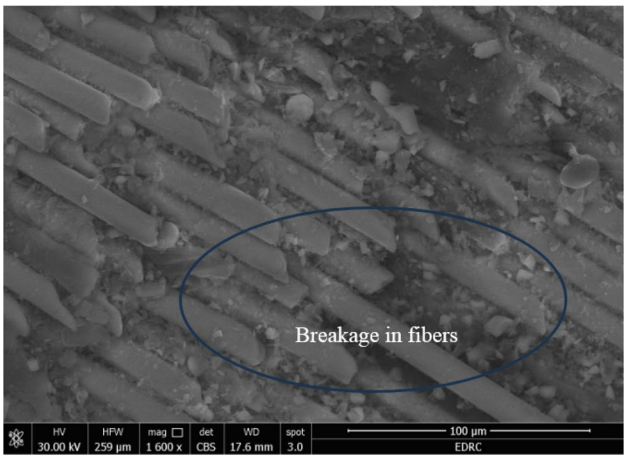


Fig. 25 SEM images of the abraded surfaces of the FRP composite (stepwise pattern) in AP-O at 40N applied load and 0.6 m/s sliding velocity for 36 m sliding distance

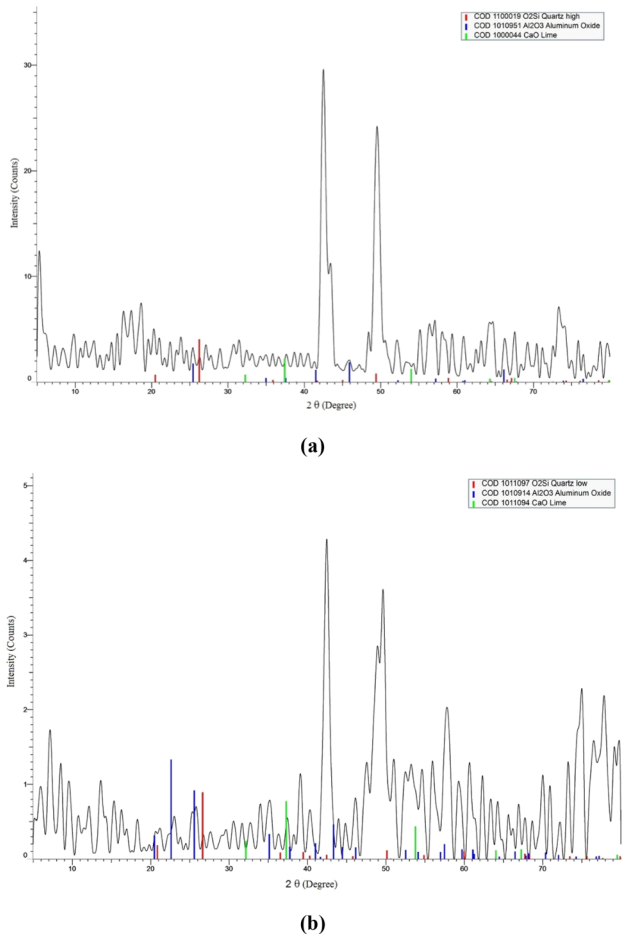


Fig. 26 XRD pattern of **a** conventional FRP and **b** linear FG-FRP after wear test

a sliding velocity of 0.6 m/s. However, the absence of fiber detachment suggests strong interfacial adhesion between the fiberglass fibers and the matrix, as further indicated by the initial occurrence of fiberglass breakage. In contrast, fiber debonding, bending, and eventual detachment occurred when composites were tested in AP-O under the same conditions, as shown in Fig. 25. This is primarily due to the side force exceeding the interfacial adhesion in the AP-O orientation.

Figure 26 presents the XRD patterns for conventional and linear FG-FRP composites after the wear test. In conventional FRP, the most prominent peaks appeared at 42.499° and 49.538°(2θ), Fig. 26a. Furthermore, the primary peaks in the linear FG-FRP pattern were observed at 42.438° and 49.619°(2θ), Fig. 26b. The crystallinity values were 42.9% for conventional FRP and 52.7% for linear FG-FRP, indicating an effective integration of long glass fibers into the epoxy resin compared to the crystallinity values obtained before and after the wear test. Some impurities (SiO_2 and Al_2O_3) were noticed due to friction with the abrasive papers. The appearance of several peaks through the XRD image may be due to the tearing and breaking of fiber and disengagement between matrix and fiber when friction with abrasive papers. This can also be noted in Fig. 20a, d.

4 Conclusions

From the obtained results, the following conclusions can be drawn.

1. At a constant PV factor, the specific wear rate is susceptible to change in the contact areas. So, a search should be made to neutralize this factor.
2. The hardness of the composites is affected by the measuring direction and redistribution of fibers at a constant volume fraction across the width of the specimens. N-O orientation exhibited higher hardness than those with the P-O and AP-O orientations. Linear distribution improves the hardness in N-O orientation, while the stepwise distribution increases it in the P-O and AP-O orientation.
3. The tribological behavior of the present laminated polymeric composite materials is greatly affected by the orientation of the fibers. Normal orientation showed superior wear resistance over the two other orientations. Linear distribution gives the highest wear resistance at N-O, while stepwise one improves this resistance at the two other orientations.
4. Care should be taken into consideration regarding the interface temperature of the glass fiber reinforced with epoxy when choosing the abrasive application conditions. It should be less than the temperature resistance of epoxy.
5. SEM images of the worn surfaces of the composite were predominated by micro-cracks (in N-O) and debonding (in P-O) in the fibrous regions and deformation in the resinous regions.
6. Finally, the linear patterns of FGCs may be recommended for use in the case of normal orientation, while the stepwise distribution for the two other orientations is also recommended.

Funding Open access funding provided by The Science, Technology & Innovation Funding Authority (STDF) in cooperation with The Egyptian Knowledge Bank (EKB). No funds, grants, or other support was received.

Data availability The raw/processed data required to reproduce these findings cannot be shared at this time as the data also form a part of an ongoing study.

Declarations

Conflict of interest The authors declare that they have no conflict of interest.

Ethical approval This article does not contain any studies with human participants or animals performed by any of the authors.

Open Access This article is licensed under a Creative Commons Attribution 4.0 International License, which permits use, sharing, adaptation, distribution and reproduction in any medium or format, as long as you give appropriate credit to the original author(s) and the source, provide a link to the Creative Commons licence, and indicate if changes were made. The

images or other third party material in this article are included in the article's Creative Commons licence, unless indicated otherwise in a credit line to the material. If material is not included in the article's Creative Commons licence and your intended use is not permitted by statutory regulation or exceeds the permitted use, you will need to obtain permission directly from the copyright holder. To view a copy of this licence, visit http://creativecommons.org/licenses/by/4.0/.

References

1. Zhang SW. State-of-the-art of polymer tribology. Tribol Int. 1998;31(1–3):49–60.
2. Friedrich KB, Lu ZB, Hager AM. Recent advances in polymer composites' tribology. Wear. 1995;190(2):139–44.
3. Rajesh JJ, Bijwe J, Tewari US. Influence of fillers on abrasive wear of short glass fibre reinforced polyamide composites. J Mater Sci. 2001;36:351–6.
4. Suresha B, Seetharamu S, Kumaran PS. Investigations on the influence of graphite filler on dry sliding wear and abrasive wear behaviour of carbon fabric reinforced epoxy composites. Wear. 2009;267(9–10):1405–14.
5. Singh SB, Chawla H. Hybrid effect of functionally graded hybrid composites of glass–carbon fibers. Mech Adv Mater Struct. 2019;26(14):1195–208.
6. Schwarzer E, Holtzhausen S, Scheithauer U, Ortmann C, Oberbach T, Moritz T, Michaelis A. Process development for additive manufacturing of functionally graded alumina toughened zirconia components intended for medical implant application. J Eur Ceram Soc. 2019;39(2–3):522–30.
7. Naebe M, Shirvanimoghaddam K. Functionally graded materials: a review of fabrication and properties. Appl Mater Today. 2016;1(5):223–45.
8. Devendrappa SK, Puttegowda M, Nagaraju SB. Enhancing wear resistance, mechanical properties of composite materials through sisal and glass fiber reinforcement with epoxy resin and graphite filler. J Indian Chem Soc. 2024;101(10):101349.
9. Pradhan S, Sahu SK, Pramanik J, Badgayan ND. An insight into mechanical & thermal properties of shape memory polymer reinforced with nanofillers; a critical review. Mater Today Proc. 2022;1(50):1107–12.
10. Dhar Badgayan N, Kumar Sahu S, Samanta S, Rama Sreekanth PS. Assessment of bulk mechanical properties of HDPE hybrid composite filled with 1D/2D nanofiller system. Mater Sci Forum. 2018;917:12–6.
11. Sahu SK, Sreekanth PSR. Artificial neural network for prediction of mechanical properties of HDPE-based nanodiamond nanocomposite. Porrimer. 2022;46:614–20.
12. Pradeep V, Kumar P, Reddy IR. Investigation on mechanical properties and wear behavior of basalt fiber and SiO_2 nanofillers reinforced composites. Results Eng. 2024;1(23):102722.
13. Saleh B, Ma A, Fathi R, Radhika N, Ji B, Jiang J. Wear characteristics of functionally graded composites synthesized from magnesium chips waste. Tribol Int. 2022;1(174):107692.
14. Song S, Zhu Z, Du S, Li Y, Liu C. Research on polymer wear under water conditions: a review. Lubricants (2075-4442). 2024;12(9):312.
15. Rajendran C, Saiyathibrahim A, Velu R. Influence of B4C and ZrB2 reinforcements on microstructural, mechanical and wear behaviour of AA 2014 aluminium matrix hybrid composites. Defence Technol. 2024;40:242–54.
16. Mohan N, Natarajan S, KumareshBabu SP. Investigation on two-body abrasive wear behavior of silicon carbide filled glass fabric-epoxy composites. J Miner Mater Charact Eng. 2010;9(03):231.
17. Chairman CA, Thirumaran B, Babu SK, Ravichandran M. Two-body abrasive wear behavior of woven basalt fabric reinforced epoxy and polyester composites. Mater Res Express. 2020;7(3):035307.
18. Suresha B, Kumar KN. Investigations on mechanical and two-body abrasive wear behaviour of glass/carbon fabric reinforced vinyl ester composites. Mater Des. 2009;30(6):2056–60.
19. Alshammaria FZ, Saleha KH, Yousif BF, Alajmib A, Shalwanc A, Alotaibib JG. The Influence of fiber orientation on tribological performance of jute fiber reinforced epoxy composites considering different mat orientations. Tribol Ind. 2018;40:335–48.
20. Dwide U, Chand N. Influence of fiber orientation on friction and sliding wear behavior of jute fiber reinforced polyester composites. Appl Compos Mater. 2009;16:93–100.
21. Zhang G, Rasheva Z, Schlarb AK. Friction and wear variations of short carbon fiber (SCF)/PTFE/graphite (10 vol.%) filled PEEK: effects of fiber orientations and nominal contacts pressure. Wear. 2010;268:893–9.
22. Manu Prasad MP, Vinod B, Sudev LJD. Effect of fiber orientation on tribological be behavior of PALF reinforced bishenol-a composite. Int J Eng Res Gen Sci. 2014;2:809–14.
23. Şahin Y, Tokdede A, Aktaş M. The effect of fiber orientation on the dry wear behavior of carbon fiber reinforced epoxy composites. J Int Sci Publ. 2017;11:317–22.
24. Chin C, Yousif B. Potential of kenaf fibers as reinforcement for tribological applications. Wear. 2009;267:1550–7.
25. Yamamoto Y, Takashima T. Friction and wear of water lubricated PEEK and PPS sliding contact part 2, composite with carbon or glass fiber. Wear. 2004;257:181–9.
26. Gautam V, Kumar A, Sharma A, Kumar D. Tribological behaviour of hybrid reinforced vinyl ester based functionally graded materials. Mater Today Proc. 2021;1(44):4682–8.

27. Singh T, Gangil B, Singh B, Verma SK, Biswas D, Fekete G. Natural-synthetic fiber reinforced homogeneous and functionally graded vinylester composites: effect of bagasse-Kevlar hybridization on wear behavior. J Market Res. 2019;8(6):5961–71.
28. Jojith R, Sam M, Radhika N. Recent advances in tribological behavior of functionally graded composites: a review. Eng Sci Technol Int J. 2022;1(25):100999.
29. Tsukamoto H. Tribological characterization of carbon nanotube/aluminum functionally graded materials fabricated by centrifugal slurry methods. J Compos Sci. 2021;5(10):254.
30. Gangil B, Patnaik A, Kumar A, Kumar M. Investigations on mechanical and sliding wear behaviour of short fibre-reinforced vinylester-based homogenous and their functionally graded composites. Proc Inst Mech Eng Part L J Mater Des Appl. 2012;226(4):300–15.
31. Singh AK, Siddhartha. Mechanical and thermo-mechanical peculiarity of functionally graded materials-based glass fiber-filled polybutylene terephthalate composites. J Reinforced Plast Compos. 2018;37(6):410–26.
32. Boggarapu V, Sreekanth PR, Peddakondigalla VB. Microstructure, mechanical and tribological properties of Al/Cu functionally graded material fabricated through powder metallurgy. J Eng Res. 2024;12(3):502–10.
33. Prakash V, Majhi S, Acharya SK. Effect of stacking sequence on abrasive wear behavior of abaca natural fiber reinforced polymer composites hybridized with glass fiber. Mater Today Proc. 2023. https://doi.org/10.1016/j.matpr.2023.02.414.
34. Alhazmi W, Jazaa Y, Althahban S, Mousa S, Abu-Sinna A, Abd-Elhady A, Sallam HE, Atta M. Mechanical and tribological behavior of functionally graded unidirectional glass fiber-reinforced epoxy composites. Polymers. 2022;14(10):2057.
35. Deshmukh KA, Chopra S, Khajanji P, Gaidhani V, Gopichand U, Gawande A, Turkar S, Khodaskar F, Deshmukh AD, Peshwe DR. Augmenting the wear performance of epoxy composites by different fillers: synthesis of highly crystalline g-C3N4 by simple pyrolysis and recycling of carbon fibres from old aircraft composites. Appl Surf Sci Adv. 2021;1(6):100125.
36. Qian G, Jian Z, Pan X, Berto F. In-situ investigation on fatigue behaviors of Ti-6Al-4V manufactured by selective laser melting. Int J Fatigue. 2020;1(133):105424.
37. Li B, Krsjak V, Degmova J, Wang Z, Shen T, Li H, Sojak S, Slugen V, Kawasuso A. Positron annihilation spectroscopy study of vacancy-type defects in He implanted polycrystalline α-SiC. J Nucl Mater. 2020;1(535):152180.
38. Askeland DR, Phulé PP, Wright WJ, Bhattacharya DK. The science and engineering of materials. 2003.
39. ASTM D3171-15. Standard test methods for constituent content of composite materials. West Conshohocken: ASTM; 2015.
40. ASTM D2240-21. Standard test method for rubber property—durometer hardness. West Conshohocken: ASTM International; 2021.
41. ASTM F732-17. Standard test method for wear testing of polymeric materials used in total joint prostheses. West Conshohocken: ASTM International; 2017.
42. Deshpande AR, Kulkarni AP, Wasatkar N, Gajalkar V, Abdullah M. Prediction of wear rate of glass-filled PTFE composites based on machine learning approaches. Polymers. 2024;16(18):2666.
43. Wei YH, Wang XL, Liu YP, Chen LJ. Effect of pin diameters on the wear characteristics of friction pairs. Strength Mater. 2019;15(51):69–75.
44. Mohankumar D, Rajeshkumar L, Muthukumaran N, Ramesh M, Aravinth P, Anith R, Balaji SV. Effect of fiber orientation on tribological behaviour of *Typha angustifolia* natural fiber reinforced composites. Mater Today Proc. 2022;1(62):1958–64.
45. Lin Z, Tao P, Zhang K, Zhao X, Gao B, Shan Z, Chen Z, Zhang Z. Regulating the severe running-in wear of polymer composites by a dual-pin-on-disk (DPOD) multicomponent approach. Wear. 2024;15(554):205483.
46. Ponnuswamy P, Manoharan M. Prediction of wear volume and friction coefficients of SS304 alloy using grey taguchi-based response surface methodology. Mater Res Express. 2024;11(6):066515.
47. Sharma M, Rao IM, Bijwe J. Influence of fiber orientation on abrasive wear of unidirectionally reinforced carbon fiber–polyetherimide composites. Tribol Int. 2010;43(5–6):959–64.
48. Korku M, İlhan R, Feyzullahoğlu E. Investigation of effects of environmental conditions on wear behaviors of glass fiber reinforced polyester composite materials. Polym Compos. 2025;46(1):355–71.
49. Zheng LY, Zhao LX, Zhang JJ. Tribological study of three-dimensionally braided carbon fiber–nylon 6 composites against 316L stainless steel. Curr Appl Phys. 2007;1(7):e120–4.

Publisher's Note Springer Nature remains neutral with regard to jurisdictional claims in published maps and institutional affiliations.

 https://doi.org/10.1007/s43452-025-01224-4

Authors and Affiliations

Mostafa A. A. Nowier[1] · Amr A. Abd-Elhady[1] · Hossam El-Din M. Sallam[2] · Mahmoud Atta[3]

✉ Hossam El-Din M. Sallam
hem_sallam@zu.edu.eg; hem_sallam@yahoo.com

Mostafa A. A. Nowier
Mostafa_Nowier@m-eng.helwan.edu.eg

Amr A. Abd-Elhady
amr_abdelfattah@m-eng.helwan.edu.eg

Mahmoud Atta
matta767@gmail.com

[1] Mechanical Design Department, Faculty of Engineering - Mataria, Helwan University, Cairo 11718, Egypt

[2] Materials Engineering Department, Zagazig University, Zagazig 44519, Egypt

[3] Mechanical Design and Production Engineering Department, Zagazig University, Zagazig 44519, Egypt